HHS Public Access

Author manuscript

Exp Neurol. Author manuscript; available in PMC 2023 July 01.

Published in final edited form as:

Exp Neurol. 2022 July ; 353: 114070. doi:10.1016/j.expneurol.2022.114070.

Rabphilin3A reduces integrin-dependent growth cone signaling to restrict axon regeneration after trauma

Yuichi Sekine[1,2],

Ramakrishnan Kannan[1],

Xingxing Wang,

Stephen M. Strittmatter[*]

Cellular Neuroscience, Neurodegeneration, Repair, Departments of Neurology and of Neuroscience, Yale University School of Medicine, New Haven, CT 06536, USA

Abstract

Neural repair after traumatic spinal cord injury depends upon the restoration of neural networks *via* axonal sprouting and regeneration. Our previous genome wide loss-of-function screen identified Rab GTPases as playing a prominent role in preventing successful axon sprouting and regeneration. Here, we searched for Rab27b interactors and identified Rabphilin3A as an effector within regenerating axons. Growth cone Rabphilin3a colocalized and physically associated with integrins at puncta in the proximal body of the axonal growth cone. In regenerating axons, loss of Rabphilin3a increased integrin enrichment in the growth cone periphery, enhanced focal adhesion kinase activation, increased F-actin-rich filopodial density and stimulated axon extension. Compared to wild type, mice lacking Rabphilin3a exhibited greater regeneration of retinal ganglion cell axons after optic nerve crush as well as greater corticospinal axon regeneration after complete thoracic spinal cord crush injury. After moderate spinal cord contusion injury, there was greater corticospinal regrowth in the absence of Rph3a. Thus, an endogenous Rab27b - Raphilin3a pathway limits integrin action in the growth cone, and deletion of this monomeric GTPase pathway permits reparative axon growth in the injured adult mammalian central nervous system.

[*]Corresponding author. Stephen.strittmatter@yale.edu (S.M. Strittmatter).

Author contributions

Yuichi Sekine: Conceptualization, Methodology, Investigation, Writing - original draft. **Ramakrishnan Kannan:** Conceptualization, Methodology, Investigation, Writing - review and editing. **Xingxing Wang:** Conceptualization, Methodology, Investigation, Writing - review and editing. **Stephen M. Strittmatter:** Conceptualization, Writing - original draft, Project adminstration, Funding Acquisition, Resources, Supervision.

[1]These authors contributed equally.

[2]Present address: Department of Cell Biology, Kyoto Pharmaceutical University, 1 Misasagi-Shichono, Yamashina, Kyoto, 607–8412, Japan.

Appendix A. Supplementary data

Supplementary data containing Figures S1 through S11 for this article can be found online at https://doi.org/10.1016/j.expneurol.2022.114070.

Declaration of Competing Interest

All other authors declare they have no competing interests.

Keywords

Axon regeneration; Rab GTPase; Rabphilin3; Integrin; Focal adhesion kinase; Spinal cord injury

1. Introduction

After adult mammalian CNS trauma, including spinal cord injury (SCI), the degree of neural recovery is limited. Even when most neurons survive, as in SCI, the restoration of neural networks is minimal because this requires axonal sprouting and/or regeneration, both of which are nil in the adult mammalian brain and spinal cord. The limitations to axonal growth are both extrinsic and intrinsic, cell autonomous and non-autonomous. Extrinsic inhibitors include glia-derived proteins, such as chondroitin sulfate proteoglycans from reactive astrocytes (McKeon et al., 1991; Shen et al., 2009) and oligodendrocyte derived proteins, Nogo, MAG and OMgp (Chen et al., 2000; GrandPre et al., 2000; Kottis et al., 2002; Liu et al., 2002; Schwab and Strittmatter, 2014). The latter three proteins are ligands for axonal NgR1 (Fournier et al., 2001; Schwab and Strittmatter, 2014), and blockade of this system with decoy receptor promotes axonal growth and functional recovery in rodent and non-human primate SCI models, both acutely and long after injury (Fournier et al., 2002; Ji et al., 2005; Lee et al., 2004; Li et al., 2005; Li et al., 2004; Wang et al., 2006; Wang et al., 2011; Wang et al., 2014; Wang et al., 2020). This therapeutic approach is now being tested in a double-blinded randomized clinical trial (ClinicalTrials.gov NCT03989440).

The role of intrinsic axonal growth determinants has also become clear. Amongst neuronal proteins, the mTOR/PTEN signaling cascade, JAK-Stat cytokine signaling and KLF transcription factors are amongst the pathways with documented roles in titrating the degree of axonal growth after injury in the adult CNS (Moore et al., 2009; Park et al., 2008; Smith et al., 2009). Furthermore, modulation of both actin and microtubule based cytoskeletal elements participate in determining the extent of axon regeneration (Ruschel et al., 2015; Tedeschi et al., 2019). To provide a more comprehensive understanding of cell autonomous regulators of axonal regeneration we completed a genome-wide loss-of-function screen in primary neuronal culture (Sekine et al., 2018). Our subsequent experiments demonstrated that *in vivo* suppression of dozens of these genes yielded axon regeneration *in vivo* after optic nerve crush by both gene silencing and gene editing methods (Lindborg et al., 2021). Amongst the 500 genes whose suppression increased axon regeneration, the Rab GTPase family was the most prominent statistically (Sekine et al., 2018). In particular, we showed that loss of Rab27b, and related Rab3 proteins, increased axonal regeneration. Moreover, mice lacking Rab27b had greater axon growth after optic nerve crush and after spinal cord hemisection (Sekine et al., 2018). However, the basis for Rab GTPase suppression to promote axon regeneration was not defined in these studies.

Here, we sought to understand the basis for Rab GTPases limiting axon regeneration. The most prominent Rab27b-interacting protein in relevant tissue was Raphilin3a (Rph3a). Moreover, gene knock-down or deletion of Rph3a yielded greater axon regeneration in cortical cultures. In regenerating axons, Rph3a co-localized with vesicle markers and Rph3a puncta associated with integrin subunits at the growth cone base, an association that was

strongly increased by axotomy. Deletion of Rph3a increased peripheral growth cone integrin levels, stimulated local focal adhesion kinase activity, and promoted F-actin filopodia in the growth cone. Moreover, increased regeneration by Rph3a null axons requires ß1-integrin. Mice without Rph3a regenerate greater numbers of regrowing retinal ganglion cell axons after optic nerve crush and corticospinal axons after either spinal cord complete crush or moderate contusion injury. Thus, Rab/Rph3a internalization of integrin receptors prevents axon growth and neural repair after spinal cord trauma.

2. Materials and methods

2.1. Mice

All animal studies were conducted with approval of the Yale Institutional Animal Care and Use Committee, The Rph3a null mice were obtained from Jackson Laboratory (B6;129P2-Rph3atm1Sud/J mice, Stock Number: 006374) (Schlüter et al., 1999). The colony was maintained with crosses to C57Bl6J mice. Initial *Rph3a*$^{-/-}$ experiments utilized littermate controls to avoid any potential strain issues until 9 backcrosses to C57Bl6J were completed. The *Rab27b*$^{-/-}$ mice have been described (Tolmachova et al., 2007). All mice were maintained on a 12 h light-dark schedule with access to standard mouse chow and water *ad libitum*. Both male and female mice were included as mice were collected from sequential littermates of the appropriate genotypes in tissue culture experiments. Spinal cord injury studies were performed only with female mice to facilitate bladder management. The male mice were used of optic nerve crush studies. The age of mice is specified in each Figure legend, and for CNS injury was introduced at 8 weeks age.

2.2. Primary cortical neuron culture and cortical axon regeneration assay

Primary cortical cultures were established from E17 C57BL/6 mice or *Rph3a*$^{-/-}$ mice. Cortices were dissected in ice-cold Hibernate E medium (catalog #HE-Ca; BrainBits) and incubated in digestion HBSS medium containing 30 U/ml Papain (catalog #LS003127; Worthington Biochemical), 1.5 mM $CaCl_2$, 2.5 mM EDTA, and 2 mg/ml DNaseI (catalog #DN25; SIGMA) at 37 °C for 20 min. Digested tissues were triturated and suspended in Neurobasal-A. Cells were plated on 96 well tissue culture plates coated with poly-D-lysine at a density of 2.5×10^4 cells per well in 200 µl of Neurobasal-A media supplemented with B-27, GultaMAX, and penicillin-streptomycin (all from Invitrogen). Cortical axon regeneration assay was performed as described previously (Huebner et al., 2011). On DIV8, 96-well cultures were scraped using a floating pin tool with FP1-WP pins (V&P Scientific) and allowed to regenerate for another 48–60 h before fixing with 4% paraformaldehyde. Regenerating axons in the scrape zone were visualized using an antibody against βIII tubulin (1:2000, mouse monoclonal; catalog #G712A; Promega). Growth cones were visualized by staining for F-actin using rhodamine conjugated phalloidin (1:2000, catalog #R415, Life Technologies). Cell density was visualized using nuclear marker DAPI (0.1 µg/ml, catalog #4083, Cell Signaling Technology). Images were taken on a 10× objective in an automated high-throughput imager (ImageXpress Micro XLS, Molecular Devices) under identical conditions. Regeneration zone identification, image thresholding and quantitation were performed blind to conditions in Image J for general regeneration assay or using an automated MATLAB script for screening. While the plates

were coated with poly-D-lysine only, the high-density cultures containing neurons and other cell types produce matrix components over the culture period. Specifically, laminin was detected immunohistochemically on the surface of culture dishes (Kannan and Strittmatter, unpublished observations).

2.3. Transfection

Cortical neurons were transfected using Amaxa mouse neuron nucleofector kit according to the manufacture's protocol. Before to plate, the dissected 4×10^6 cortical neurons were resuspended in 100 μl of nucleofector solution and mixed with 5 μg of plasmids. Then neurons were nuculeofected using the program O-005 and plated on PDL-coated 96 well plate for regeneration assay, 6 well plate for immunoprecipitation, 24 well plate for western blot or 8 well glass chamber slide for confocal imaging.

2.4. Time-lapse imaging of regenerating axons

For imaging studies, six million cortical neurons were transfected with 2 μg of cytosolic FAK biosensor for FRET imaging and LifeAct-mScarlet for imaging actin dynamics. The neurons were seeded in cover-glass bottom m-dish 35 mm Ibidi culture dishes with Neurobasal medium and supplements at 37 °C + 5% CO_2 maintained imaging chamber in Zeiss LSM 880, Airyscan module for all time-lapse experiments. Axotomy was performed mechanically as for the 96-well plate experiments above. The coverslips were precoated sequentially with poly-L-lysine (Invitrogen; P5899 at 50 μg/ml) and Laminin (Gibco; 23,017–015 at 50 μg/ml). Fresh media was added before each imaging session. *Z*-stacks were acquired every 2 min for total 24–30 min total. Morphometric analysis of filopodia performed using FiloQuant software (Jacquemet et al., 2019) with *z*-MIP across time scale by a researcher unaware of the experimental group.

2.5. Cytosolic FAK biosensor imaging

Ratiometric FRET imaging was performed as described previously (Kannan et al., 2017). Argon 405 nm laser line in Zeiss LSM 880 system was used to excite eCFP (433 nm) and collect emission at 527 nm (FRET) and 476 nm (ECPF alone), respectively. ~12–15 *z*-stacks with 1024 × 1024 frame size were acquired using 63 × 1.42 NA objective lens at 2 × zoom. All measurements were analyzed from *z*-projection image. Region of interest (ROIs) were manually drawn in MetaMorph (Molecular Devices) and respective average intensity values in ECFP (I_{cfp}) and FRET (I_{fret}) were used for further analysis. For background subtraction (I_{bg}), average intensity values for both CFP and FRET channel were measured for each image. FRET ratio (R_f) was calculated using this formulae $R_f = (I_{cfp}\text{-}I_{bg\text{-}cfp})/(I_{fret}\text{-}I_{bg\text{-}fret})$ Pixel-by-pixel ratio images of ECFP/YPet were generated based on the background deducted fluorescence intensity images of ECFP and YPet in MetaMorph software. The ratio images are displayed in the intensity modified display mode, where the colour and brightness of each pixel is determined by ECFP/YPet ratio images.

2.6. Integrin function blocking assay in cortical neurons

To block endogenous ß1-integrin signaling in cultured neurons, 2.5 μg/ml of anti-ß1-integrin antibody (BD Biosciences; Cat No: 555003, Clone Ha2/5) was added immediately after

scrape injury, similar to its use in previous outgrowth assays (Hu and Strittmatter, 2008). These cultures were compared with those treated in parallel with IgM λ1 isotype control antibody (BD Biosciences; Cat No: 553958, Clone G235–1).

2.7. Immunoprecipitation, silver staining and mass spectrometry

DIV 10 neurons were lysed with a RIPA buffer (50 mM Tris-HCl pH 7.4, 150 mM NaCl, 1 mM EDTA, 0.1% SDS, 0.5% sodium deoxycholate and 1% Triton X-100) and centrifuged at 20,000 x*g* for 20 min at 4 °C. The supernatants were added with the antibody and protein G-sepharose mixture and incubated for 2 h at 4 °C with gentle rotation. The beads were washed three times and the immune complexes were then resolved by SDS-PAGE. For mass spectrometry, the gel was stained by Silver Stain MS kit (Wako, #299–58,901) according to manufacturer's instruction, and the bands were excised and subjected to analysis by mass spectrometry (the MS and Proteomics Resource of the WM Keck Foundation Biotechnology Resource Laboratory at Yale University).

2.8. Immunoblotting

Cell lysate or immunoprecipitated samples were resolved by SDS-PAGE and transferred to nitrocellulose membranes. Then, they were incubated in blocking buffer (Blocking Buffer for Fluorescent Western Blotting, Rockland MB-070-010) for 1 h at RT and immunoblotted with the appropriate primary antibodies. Following primary antibody incubation, secondary antibodies (Odyssey IRDye 680 or 800) were applied for 1 h at RT. Membranes were then washed and visualized using a Licor Odyssey Infrared imaging system.

2.9. Expression plasmids

FLAG-tagged Rab27b WT, T23N and Q87L mutants have been previously described (Sekine et al., 2018). Wild-type mouse-Rph3a-DYK (#OMu14590D) purchased from GenScript was subcloned into pAAVCAG-GFP vector using BamHI/*Eco*RI digestion and used for generating mutant constructs by PCR-methods using KOD Hot start DNA polymerase (TOYOBO, Japan) and sequenced. pAAV-U6-GFP Expression Vector (#VPK-413, Cell Biolabs) was used for making shRNA constructs. Targeting shRNA sequences are shNC:TTCTCCGAACGTGTCACGT, shRph3a#1:CATTGGCAAGTCTAATGATTA, shRph3a#2:GACATTGGCAAGTCTAATGAT, shMADD#1: CCACAAGTACAAGACGCCAAT, shMADD#2: GCCCATCCATTATCGAGTCTA, and shRab3c#1: CGATTCCTTTACATCTGCATT. The FRET biosensor for FAK has been described(Cai et al., 2008). The LifeAct-mScarlet plasmid was obtained from Addgene (#85056).

2.10. Immunological reagents

The following antibodies were used: Mouse monoclonal anti-βIII-Tubulin antibody, Promega, #G7121; Rabbit polyclonal anti-Rab27b antibody, Immuno-Biological Laboratories, #18973; Rabbit polyclonal anti-FLAG antibody, Sigma-Aldrich, #F7425; Mouse monoclonal anti-β-Actin antibody, Sigma-Aldrich, #A1978; Mouse monoclonal anti-GFAP antibody, Sigma-Aldrich, #G3893 Goat polyclonal anti-Rph3a antibody, Santa

Cruz Biotechnology, #sc-14,678; Mouse monoclonal anti-GFP antibody, Santa Cruz Biotechnology, #sc-9996; Rabbit monoclonal anti-MADD[EPR4919] antibody, abcam, #ab134117; Rabbit polyclonal anti-Rab3c antibody, abcam, #ab3336; Rabbit polyclonal anti-5HT antibody, Immunostar, #20080; Donkey anti-mouse IgG Alexa Fluor 488, Thermo Fisher Scientific, #A21202; Donkey anti-mouse IgG Alexa Fluor 647, Thermo Fisher Scientific, #A31571; Donkey anti-rabbit IgG Alexa Fluor 488, Thermo Fisher Scientific, #A21206;IRDye 680 Donkey anti-Mouse IgG (H + L), Li-Cor, #926–68,072; IRDye 680 Donkey anti-Rabbit IgG (H + L), Li-Cor, #926–68,073; IRDye 800 Donkey anti-Rabbit IgG (H + L), Li-Cor, #926–32,213; IRDye 800 Donkey anti-Goat IgG (H + L), Li-Cor, #926–32,214; Streptavidin Alexa Fluor 568, Thermo Fisher Scientific, #S11226; Rhodamine Phalloidin, Thermo Fisher Scientific, #R415; Alexa fluor 488 Phalloidin, Thermo Fisher Scientific, #A12379; Anti-FAK Millipore 05–537, Clone 4.47; anti-phospho-Tyr397-FAK, Sigma, ABT135; antβ1-integrin BD Biosciences, 555,003, Clone Ha2/5; IgM λ1 isotype control antibody, BD Biosciences, 553,958, Clone G235–1.

2.11. Coimmunoprecipitation

Tissue was collected from 7d post-axotomy *in vitro* cortical neurons, optic nerve, and thoracic region of spinal cord. Samples were briefly sonicated in RIPA buffer and centrifugation at 14,000 x*g* for 15 min at 4 °C. Immunoprecipitation was performed by mixing 40 μg of supernatant protein with 2–3 μg of control IgG or anti-Rph3a overnight at 4 °C with constant rotation. Proteins were immunoprecipitated with protein G-conjugated agarose beads by constant rotation for 3 h at 4 °C. Immunocomplexes with the beads were washed thrice in 1% NP-40 buffer containing phosphatase and protease inhibitors. Precipitated proteins were analyzed by immunoblot using anti-ß1-Integrin and ß-actin with appropriate internal controls.

2.12. Immunocytochemistry

At DIV 8 neurons were scraped with pipet tip and allowed for 2 days to regenerate. Then, cells were fixed with 4% paraformaldehyde for 15 min, and then permeabilized with 0.1% Triton X-100 in PBS for 15 min. Regenerating axons in the scrape zone were visualized using an antibody against βIII tubulin (1:2000, mouse monoclonal; catalog #G712A; Promega). FLAG-Rph3a was stained with anti-FLAG (1:1000, Sigma-Aldrich, #F7425) antibody. Then, either Alexa-488 or Alexa-568 conjugated donkey anti-rabbit IgG and Alexa-647 conjugated donkey anti-mouse IgG (1:2000, all from Invitrogen) were used to detect primary antibodies. Growth cones were visualized by staining for F-actin using Alexa-488- or rhodamine-conjugated phalloidin (1:2000, catalog #A12379 or #R415, Life Technologies). Samples were mounted with mounting solution (Vector Laboratories) and observed using a LSM710 confocal microscope with 63× objection lens.

2.13. Mice and surgery

All surgery, animal handling, behavioral measures and tissue collection was completed by personnel unaware of genotype. All procedures and postoperative care were performed in accordance with the guidelines of the Institutional Animal Use and Care Committee at Yale University.

Optic nerve crush experiments utilized 12-week-old littermate-matched WT or *Rph3a*$^{-/-}$ mice F1 offspring from *Rph3a*$^{+/-}$ crosses with equal numbers of male and female in each group. The animals were anesthetized by intraperitoneal injection of ketamine (100 mg/kg) and xylazine (10 mg/kg). Topical 2% lidocaine anesthetic was applied to the eyeball. The optic nerve was exposed intraorbitally with care taken to avoid damage to the ophthalmic artery. The nerve was injured by crushing with a jeweler's forceps (Dumont 5; Fine Science Tools) for 5 s at a location 1 mm posterior to the eyeball (Wang et al., 2015). Alexa-555-Cholera toxin beta (CTB) was injected intravitreally to trace retinal ganglion cell axons 14 days after injury. Three days after the tracing, animals were sacrificed and dissected the optic nerves.

Age- and littermate-matched 6-week-old female *Rph3a*$^{+/-}$ or *Rph3a*$^{-/-}$ mice were subjected to spinal cord complete crush injury as described previously (Zhang et al., 1996; Zukor et al., 2013) with modifications. At the time of the experiment, the strain had been backcrossed to the C57BL/6 WT 6 times (F6). All animals received subcutaneous injection of buprenex (0.01 mg/kg) 30 min before surgery and were deeply anesthetized with ketamine (100 mg/kg) and xylazine (15 mg/kg). To expose the spinal cord from side-to-side at T7 levels, laminectomy was performed keeping the dura intact. The spinal cord was then completely crushed for 3 s with Dumont #5 forceps that had been filed to 0.2 mm width. Muscle and skin overlying the lesion were sutured. All animals received subcutaneous injection of 100 mg/kg ampicillin and 0.1 mg/kg buprenex twice a day for the first two days after surgery, and additional injections later as necessary.

For mouse spinal contusion injury, age-matched 6-week-old female *Rph3a*$^{-/-}$, *Rph3a*$^{+/-}$ or WT C57BL/6 mice were subjected to spinal cord contusion injury by utilizing Infinite Horizon impactor (IH-0400 impactor, Precision Systems and Instrumentation, LLC, VA, USA). At the time of the experiment, the mice had been backcrossed to the C57BL/6 WT greater than 9 times (F9) and were not littermate-matched. Mice were anesthetized with intraperitoneal injection of ketamine and xylazine as described in the mice spinal crush injury. A dorsal midline incision was made over the thoracic spinal cord. A complete laminectomy was made at T9 vertebral level with the dura intact. The mice were stabilized with forceps positioned along the lateral processes of T8 and dorsal process of T10. The contusion injury was induced by applying a force of 70 kdyn through the impactor to the exposed spinal cord. Overlying muscle layers and skin were sutured. Post-operative care was similar to the mice received spinal cord crush injury.

2.14. Behavioral tests

Behavioral tests were performed unaware of the genotype of the mice. For mouse behavioral observation, the Basso Mouse Scale (BMS) was used as a measure of open-field locomotion (Basso et al., 2006), which has a quantitative scale from 0 to 9. Animals were tested 3 d before injury for baseline function and 3, 7, 28, 42, 56, 70 and 84 d post lesion (dpl).

2.15. Histology and immunohistochemistry

All tissue collection, staining and axon measurement was completed by personnel unaware of genotype.

Mice were euthanized and transcardially perfused with cold PBS followed by 4% paraformaldehyde. Spinal cords were dissected, postfixed in 4% paraformaldehyde at 4 °C, and subsequently embedded in 10% gelatin. Serial sections (40 μm) were collected on a vibratome (VT1000S, Leica). Transverse sections were collected at cervical enlargements and lumbar enlargements. Thoracic lesion site (from −5 mm rostral to +5 mm caudal) was excised from each animal and sectioned sagittally, collecting every single section. Sections of spinal cord were blocked and permeabilized with 10% normal donkey serum and 0.3% Triton X-100 in PBS for 1 h. Then, sections were incubated with 5-HT (1:1000) or anti-GFAP (1:1000) antibody and visualized with Alexa-488 conjugated secondary antibody (1:1000). The images were taken by the Zeiss LSM710 confocal microscope and analyzed by using National Institutes of Health (NIH) ImageJ 1.49v, as described previously (Wang et al., 2014). For analysis of serotonin innervation, immunoreactive serotonin fibers in the ventral horn of transverse sections were selected by thresholding, and then the intensity of serotonin fiber per area was measured after using the “skeletonize” function.

For optic nerve (ON) crush experiments, the ON was dissected from the eyeball and postfixed in the 4% PFA solution. After clearing the whole nerve (Erturk et al., 2011), the sample was mounted on a glass side with a coverslip for imaging. For ON axon quantification, the ON was imaged by using the Zeiss LSM 710 confocal microscope with 20× objective lens. Axons labeled with CTB (Cholera Toxin Subunit B Alexa Fluor 555 Conjugate, Thermo Fisher Scientific, #C34776) were counted from the different distances to the crush lesion. Total number of regenerating axons was counted from each image in 30–40 section *Z*-stacks.

To trace the CST after spinal cord complete crush, biotin dextran amine (BDA, Dextran Biotin 10,000 MW Lysine Fixable (BDA-10,000, Thermo Fisher Scientific, # D1956) was injected bilaterally into the sensorimotor cortex. In each animal, 150 nl of 10% solution of BDA was injected at each of the six sites (coordinates from bregma in mediolateral/anterior–posterior format in mm: 1.0/0.0, 1.5/0.5, 1.5/0.5, 1.5/1.0, 1.0/−1.5, 1.5/−0.5) for a total of 900 nl volume per hemisphere. Two weeks after the tracing, animals were killed by transcardial perfusion with PBS followed by 4% PFA. To trace the CST after spinal contusion, AAV-RFP tracer virus was injected bilaterally into the sensorimotor cortex. (pENN.AAV.hSyn.TurboRFP.WPRE.RBG, Addgene #105552-AAV1).

CST axons were counted in sagittal sections of the thoracic spinal cord spanning the lesion as the number of fibers crossing a dorsal-ventral lines at defined distances rostral and caudal to the injury center and all sections spanning the spinal cord. CST axons were also counted in transverse sections of the spinal cord at C1 level to capture the total number of labeled fibers.

The values collected from sections spanning the lesion site were converted to a CST Fiber Index as a ratio to the total number of labeled fibers counted rostrally, such that 1.0 would equal a count identical to the rostral count for that mouse. For the crush injury of Fig. 8, the CST axon count at 500 μm was taken as 100%, while in the contusion experiment of Fig. 10, the CST axon count in transverse C1 sections was taken as 100%.

2.16. Statistical analysis

One-way ANOVA with post-hoc Tukey pairwise comparisons, Repeated Measures ANOVA, Fisher's Exact test, and Student *t*-test as specified in the Figure legends were performed using GraphPad Prism (version 5.0d) or SPSS Statistics (v26). Means ± sem and specific n values are reported in each Figure legend. Data are considered statistically significant if $p \leq 0.05$. All tests were two-sided. The assumption of Gaussian distribution was checked using D'Agostino-Pearson omnibus test.

3. Results

3.1. Identification of Rab27b effector as Rph3a

Previously, we completed a genome-wide loss-of-function screen for factors limiting axonal regeneration after scrape axotomy by arrayed shRNA knockdown for cerebral cortical neurons *in vitro* (Sekine et al., 2018). This screen detected 500 genes whose suppression enhanced regeneration, and identified multiple specific Rab and Rab-related proteins of the intracellular transport system as being inhibitory for axonal regeneration. In particular, Rab27b limits axonal regeneration and neurological recovery after injury *in vivo* (Sekine et al., 2018). Specific effectors are required for activated GTP-bound Rab protein to mediate membrane traffic in various pathways. Multiple Rab27 effectors have been identified previously (Fukuda, 2013), and many were contained in our previous screen (Fig. S1)(Sekine et al., 2018). In Fig. 1A, the Rab27b protein interaction network related to axon regeneration is illustrated. The protein-protein interaction network of mouse proteins connected to Rab27b from the Visant website (http://visant.bu.edu). Each node in red was a regeneration hit in the primary screen (Fig. 1A). Amongst these, Rab27b is direct binding partner for Rph3a and Sytl1. To identify the relevant effector for Rab27b during axonal regeneration, we performed immunoprecipitation analysis with 1×10^5 cells cultured in 6 well dishes under the same culture conditions as used for the axon regeneration screen, and identified associated proteins by liquid chromatography - mass spectrometry (LC/MS) of tryptic peptides from SDS-PAGE protein bands. We included inactive Rab27b T32N mutant as a negative control since it is predicted to be incapable of effector interaction. Silver staining of proteins in a FLAG-Rab27b immunoprecipitate from neurons transfected with Rab27b WT reveals a 75 kDa band, which is not present in Vector or Rab27b TN precipitates (Fig. 1B). This 75 kDa band was excised, and its components analyzed. From the LC/MS analysis, we identify Rph3a as a prominent binding partner of Rab27b in cortical neurons. To confirm this binding, the Rab27b immunoprecipitates were examined by anti-Rph3a immunoblot. Consistently, Rab27b WT and the constitutively active Q78L mutant form a complex with endogenous Rph3a, but the TN mutant does not do so (Fig. 1C). We also confirmed the interaction between endogenous Rab27b and Rph3a in primary cortical neurons (Fig. 1D). We conclude that Rph3a is the principal partner of Rab27b in growing axons.

3.2. Rph3a suppresses axonal regeneration in vitro

To determine whether Rph3a has a function in axonal regeneration, we utilized Rph3a shRNA constructs in the cortical neuron scrape assay. Endogenous Rph3a expression is reduced by more than 80% after shRph3a transfection (Fig. S2A). Importantly, axon

regeneration measured as ßIII-tubulin immunoreactive area in the scrape zone is significant greater after Rph3a knockdown than in shNC controls ($p < 0.01$, one-way ANOVA) (Fig 2A and B). *Rph3a* deletion mice are viable (Schlüter et al., 1999), so we cultured *Rph3a*$^{-/-}$ cortical neurons. Consistent with the shRNA data, axonal regeneration from *Rph3a*$^{-/-}$ mouse neurons is enhanced significantly relative to WT ($p < 0.005$) (Fig. 2C, D and S2B). Therefore, Rph3a interacts with Rab27b and regulates axon regeneration in cortical neurons.

3.3. Signaling cascade of Rph3a-mediating axonal regeneration

Generic Rab activity is regulated by cycle between a GDP-bound inactive and a GTP-bound active state. Guanine nucleotide exchange factors (GEFs) function upstream to activate Rab proteins by stimulating the release of GDP and to allow binding of GTP. Since MADD (also known as DENN) is characterized as a GEF for Rab27 (Imai et al., 2013; Yoshimura et al., 2010), we examined the effect of MADD in axonal regeneration. Reduction of MADD expression by shRNA-mediated knockdown significantly enhances axonal regeneration by cortical neuron *in vitro* (Fig. S3A-C). This result suggests that MADD suppresses axonal regeneration by activating Rab27b. We sought to determine whether MADD acts specifically *via* Rab27b signaling. Knockdown of MADD in *Rab27b*$^{-/-}$ neurons has no effect on axonal regeneration, consistent with MADD acting *via* Rab27b for axon regeneration (Fig. S4A-C).

We also assessed the specificity of Rph3a function using *Rab27b*$^{-/-}$ neurons. Distinct from MADD, the reduction of Rph3a in *Rab27b*$^{-/-}$ neurons enhances axonal regeneration, by 21% (Fig. S4D-F). Rph3a was identified as a Rab3 effector for regulation of synaptic vesicle release prior to the description of its interaction with Rab27b (Geppert et al., 1994; Shirataki et al., 1992). Previously, we found that Rab3 isoforms, especially Rab3b and Rab3c, suppress axonal regeneration in the same manner as Rab27b (Sekine et al., 2018). Therefore, we assessed the role of both Rab3 and Rph3a for axonal regeneration by *Rab27b*$^{-/-}$ neurons. Rab3c reduction in *Rab27b*$^{-/-}$ neurons enhances axonal regeneration to an extent similar to Rph3a knockdown (Fig. S4G and S4H). However, double knockdown of both Rph3a and Rab3c in *Rab27b*$^{-/-}$ neurons produces no further increase in axonal regeneration relative to Rab3c single knockdown. Thus, with regard to axon regeneration, MADD appears to be a specific GEF for Rab27b, while Rph3a is an effector for both Rab27b and Rab3c.

3.4. Rph3a and integrins

A crucial aspect of Rab GTPase function is their localization to specific cell compartments. Rph3a is known to localize to the synaptic vesicles in the presynapse, as well as to postsynaptic sites in neural networks formed by mature neurons (Mizoguchi et al., 1994; Stanic et al., 2015). To investigate the cellular role of Rph3a in axon regeneration, we examined its co-localization with synaptic markers in wild type cortical neurons. The absence of anti-Rph3a signal in *Rph3a*$^{-/-}$ cultures verified antibody staining specificity. Rph3a distribution closely matched that for the *bona fide* vesicle membrane marker proteins, synaptophysin and synapsin IIb (Figs. 3A, S5A). The Pearson's correlation coefficient r for colocalization of synaptophysin and Rph3a was 0.73. Rph3a distribution did not overlap substantially with the active zone scaffolding protein, Bassoon (Fig. S5B).

Since vesicle membrane proteins have been implicated in the regulation of receptor signaling at plasma membrane prior to synapse formation during morphological remodeling after nerve injury (Eva and Fawcett, 2014), we examined the relative distribution of ß1-integrin and Rph3a vesicles in axonal growth cones under basal conditions and during regeneration after axotomy (Fig. 3B). Rph3a is detected in puncta consistent with intracellular vesicles throughout the palm of the growth cone and this is not altered during regeneration. Integrins containing the ß1 subunit are prominent in radially oriented linear arrays at the growth cone periphery consistent with adhesion complexes, while a minor component colocalizes with the Rph3a vesicular puncta more proximally in the growth cone. After axotomy, the overall levels of ß1-integrin in the growth cone decrease significantly, in contrast to unchanged Rph3a levels (Fig. 3B, C). The decrease in integrin level is specific to the peripheral radial array component, with the integrin/Rph3a-colocalized clusters remaining unchanged after axotomy (Fig. 3C). The Pearson's correlation coefficient r for colocalization of ß1-integrin and Rph3a in WT growth cones was 0.10 without injury and 0.13 with axotomy, and not significantly different. We considered whether the loss of ß1-integrin from growth cone peripheral radial arrays requires Rph3a, hypothesizing that the co-clusters might reflect active integrin endocytic structures. In *Rph3a*$^{-/-}$ cultures, axotomy fails to reorganize ß1-integrin distribution, such that the peripheral radial array remains prominent, and there is a slight increase in growth cone ß1-integrin signal (Fig. 3D). Thus, a subset of growth cone integrin associates with Rph3a puncta and the presence of Rph3a is required for integrin depletion from the growth cone after axotomy, potentially through endocytic vesicles.

If post-axotomy endocytic removal occurs by Rph3a-dependent clearance, then the association of the two proteins is predicted to increase and be detected biochemically. We assessed Rph3a immunoprecipitates isolated from the regenerating fibers in scrape-injured cortical cultures, or in the optic nerve 7 days after crush, or in that spinal cord 7 days after injury (Fig. 3E). There is a pronounced increase in Rph3a association with ß1-integrin receptors in regenerating fibers compared with uninjured controls in all three axotomy paradigms. Endogenous ß1-integrin levels remain unaltered after injury, suggesting that the increased association of ß1-integrin with Rph3a would restrict the ability of downstream integrin signaling at the plasma membrane to support axon regeneration.

The loss of the peripheral radial array of integrin receptors from WT growth cones suggests the downstream integrin signaling is reduced in WT regenerating growth cones as compared to *Rph3a*$^{-/-}$ regenerating growth cones. We monitored the activity of the cytoplasmic focal adhesion kinase (FAK), which bridges ß1-integrin to cytoskeletal remodeling. The FRET response of a FAK biosensor reports the intramolecular interaction between endogenous FAK phosphorylated substrate and the SH2 domain (Cai et al., 2008) (Fig. 4A, B). Consistently, we observe enhanced FAK biosensor activity in *Rph3a*$^{-/-}$ regenerating fibers of cortical neurons compared to WT fibers. For biochemical confirmation of this imaging result, we measured the levels of FAK (Y397) tyrosine phosphorylation compared to total FAK in protein extracts from regenerating fibers of WT and *Rph3a*$^{-/-}$ neurons. There is a substantial increase in active phospho-Y397-FAK relative to total FAK in *Rph3a*$^{-/-}$ cultures (Fig. 4C, D). Collectively, these results highlight the regulatory role of Rph3a in restricting downstream activation of integrin signaling in WT axons after axotomy.

Actin filaments, as regulated by integrins, FAK and extracellular signals, are key determinants of axonal growth cone motility and axon extension. To assess the effect of Rph3a of F-actin in regenerating axons, we expressed LifeAct fused to mScarlet and imaged in time-lapse experiments. We measured filopodia length, filopodia density and axon extension rate in WT and *Rph3a*$^{-/-}$ cortical neurons (Fig. 5A-D). Loss of Rph3a leads to substantial increases in filopodial length, filopodial density and axon extension rate. These data are consistent with Rph3a acting to remove surface ß1-Integrin complexes and thereby reduce FAK activity and F-actin-rich filopodia to restrict axonal regeneration. Growth cone area has been linked to actin polymerization, so we also measured growth cone area under these conditions (Fig. 5E). The regenerating *Rph3a*$^{-/-}$ axons show a modest increase in area relative to WT axons.

To assess the dependence of Rph3a restriction of axonal regeneration on integrin signaling, we inhibited integrin activity with function-blocking antibodies. Amongst the multiple integrin dimers, ß1 heterodimers with α5 and αv integrin subunits show widespread expression in adult brain and in axonal growth cones (Hu and Strittmatter, 2008). Here, we added a function-blocking anti-ß1-integrin antibody to axotomized cultured neurons from WT and *Rph3a*$^{-/-}$ animals (Fig. 5F-H). While the time lapse experiments included laminin precoating of the glass substrate, these multiwell regeneration experiments on plastic did not include specific coating with an integrin-interacting matrix protein but we verified the deposition of cell-derived laminin on the substratum by immunostaining (Kannan and Strittmatter, unpublished observations). Inhibition of integrin signaling blocks the increased axon regeneration measured by ßIII-tubulin length observed in isotypecontrol antibody *Rph3a*$^{-/-}$ neurons compared to WT neurons. The ability of Rph3a deletion to increase the number of regenerating F-actin-rich growth cones scored as phalloidin-positive tips per area is also eliminated by the function-blocking anti-ß1-integrin antibody. Together, these mechanistic studies reveal an injury-dependent Rph3a-mediated restriction of integrin signaling occurs in WT neurons to limit axon regeneration involving F-actin-rich filopodia.

3.5. Optic nerve axon regeneration in Rph3a$^{-/-}$ mice

Since suppression of Rph3a expression enhanced axonal regeneration *in vitro*, we evaluated the *in vivo* function of Rph3a. We utilized the optic nerve crush model of axon regeneration because Rph3a expression is observed in WT retinal tissue, but not in *Rph3a*$^{-/-}$ retina (Fig. S6). WT and *Rph3a*$^{-/-}$ mice were subjected to optic nerve crush injury and injected the anterograde tracer cholera toxin B (CTB) into the retina 14 days after crush. Animals were sacrificed and dissected to collect the optic nerves 3 days after CTB injection. CTB-labeled axons are intensely observed up to the crushed lesion in both genotypes. The total number of CTB-positive axons regenerating 200 μm or 500 μm beyond the injury site in *Rph3a*$^{-/-}$ optic nerve is significantly increased compared with WT ($p < 0.0001$ at 200 μm, $p < 0.05$ at 500 μm), whereas at 1000 μm distally the values are low and indistinguishable (Fig. 6A and B). Thus, these data show that endogenous Rph3a limits axonal regeneration *in vivo*.

3.6. Enhanced behavioral recovery in Rph3a$^{-/-}$ mice after spinal cord injury

Suppression of Rph3a expression enhanced axonal repair *in vitro* and *in vivo*, so we sought to determine whether functional recovery from traumatic spinal cord injury (SCI) might be

enhanced by *Rph3a* deletion. The *Rph3a*$^{+/-}$ and *Rph3a*$^{-/-}$ mice were received spinal cord complete crush surgery at the midthoracic level (n = 17 *Rph3a*$^{+/-}$, n = 12 *Rph3a*$^{-/-}$). These initial transection experiments utilized heterozygous littermate controls as we expanded a C57Bl6 backcrossed *Rph3a* colony, with the hypothesis that Rph3a would exert a recessive effect on neural repair phenotype. Functional recovery of the injured animals was scored using the Basso-Mouse-Score (BMS)(Basso et al., 2006). Recovery of hindlimb function is significantly improved in *Rph3a*$^{-/-}$ animals at 10 and 12 weeks after axotomy (Fig. 7A; RM-ANOVA, p = 0.039). The percentage of *Rph3a*$^{-/-}$ mice capable of bearing weight with their hindlimbs in the open field was twice as great as for heterozygous *Rph3a*$^{+/-}$ animals at day 84 (Fig. 7B; Fisher's Exact, p = 0.038).

The projection of corticospinal axons after SCI was assessed for axon regeneration. The anterograde tracer BDA was injected into sensorimotor cortex at 10 weeks post-SCI. Two weeks after tracer injection, tissue was collected and BDA tracer visualized with streptavidin Alexa Fluor 568 (Fig. 8A, S7A, S7B). Rostral to the injury, in the upper cervical cord, there was no detectable difference in the number of labeled CST axons in the *Rph3a*$^{+/-}$ and *Rph3a*$^{-/-}$ mice (Fig. S7). In heterozygous injured mice, essentially all CST axons are interrupted by the complete crush, and no fibers reached into the caudal spinal cord. The count of BDA-labeled regenerating CST axons was significantly increased from 100 μm rostral to the lesion to 300 μm caudal to the lesion in *Rph3a*$^{-/-}$ animals as compared to *Rph3a*$^{+/-}$ (Fig. 8B and C; RM-ANOVA, p = 0.001). The fiber density is approximately 1% of the fiber density 500 μm rostral to the injury site (a CST Fiber Index of 0.01). This cannot be explained by an altered developmental trajectory of CST fibers, because deletion of *Rph3a* did not alter CST trajectory for uninjured mice (Fig. S8A). Thus, deletion of Rph3a allows a limited degree of CST regeneration across a complete cord crush injury.

The raphespinal serotonergic (5HT) axonal tract has a greater capacity for injury-induced axonal growth than does that CST and is documented to contribute to rodent locomotion (Kim et al., 2004). For naïve uninjured mice, the density of spinal cord 5HT-positive fiber length is comparable for *Rph3a*$^{+/-}$ and *Rph3a*$^{-/-}$ animals (Fig. S8B and S8C). We assessed 5HT staining in the caudal ventral horn gray matter of the lumbar spinal cord for the injured cohort. The density of 5HT-positive fibers is five times greater in the *Rph3a*$^{-/-}$ group as compared to *Rph3a*$^{+/-}$ group (Fig. 9A and B). Taken together, the improved functional recovery and increased descending axonal length show that deletion of Rph3a is beneficial for neural repair after SCI.

3.7. Corticospinal axon regeneration in Rph3a$^{-/-}$ mice after spinal cord contusion

We sought to evaluate whether suppression of Rph3a would also improve repair in mice with a more translationally relevant spinal contusion injury. *Rph3a*$^{-/-}$ and WT mice underwent moderate spinal contusion injury at the T9 vertebral level (n = 7 *Rph3a*$^{-/-}$, n = 7 WT). Here, the *Rph3a*$^{-/-}$ mice were from an expanded colony after backcrossing to C57Bl6 for 9 generations. There were no statistically significant differences in spared tissue between groups (Fig. S9A, B). In this experiment, AAV-RFP was injected into sensorimotor cortex to trace CST anterogradely at 70 days after SCI, and no difference in labeling of the CST in the upper cervical cord was detected between groups (Fig. 10A, B). AAV-RFP was substituted

for BDA tracing to provide more robust tracer signal. The regenerating RFP-labeled CST axon number was significantly increased at 500 μm to 2000 μm caudal to the lesion in knockout *Rph3a*$^{-/-}$ animals as compared to control WT mice (Fig. 10). The density of CST fibers in the *Rph3a*$^{-/-}$ group was between 1 and 2% of CST fiber density in the cervical cord (a CST Fiber Index of 0.01–0.02). The CST fiber count was much lower but not zero in the control group, so the distal CST fibers in the *Rph3a*$^{-/-}$ mice may reflect a combination of regeneration and distal sprouting from the few spared fibers. Nonetheless, there are more CST fibers in the caudal spinal cord of the *Rph3a*$^{-/-}$ mice.

The hindlimb locomotor function in the open field did not show a difference between the WT and *Rph3a*$^{-/-}$ groups studied histologically (not shown). Even when combined with a larger group including heterozygous mice (n = 21 *Rph3a*$^{-/-}$, n = 13 *Rph3a*$^{-/+}$, n = 7 WT), a trend to improvement in *Rph3a*$^{-/-}$ animals *versus* control WT plus *Rph3a*$^{-/+}$ heterozygous mice failed to reach statistical significance at 70, 84 and 98 days after spinal contusion (Fig. S11). Thus, while the absence of Rph3a allowed significantly caudal CST axon growth in this model there was no detected functional benefit.

4. Conclusions

The major finding of the current study is that Rph3a is a Rab GTPase effector limiting axon regeneration in the adult mammalian CNS. After axotomy, there is increased association of Rph3a with ß1-containing integrins, and the growth-promoting effect of Rph3a loss requires the function of ß1 integrin. Without Rph3a, there is greater integrin and FAK activation with enhanced growth cone filopodia leading to axonal regeneration. Mice lacking Rph3a exhibit increased axon regeneration from retinal ganglion cells after optic nerve crush and from CST neurons after either complete spinal cord crush. After spinal cord contusive injury, there is increased CST sprouting or regeneration or both in the caudal cord. Thus, Rph3a-mediated removal of integrin receptors from the axonal growth cone limits axon regrowth and repair after traumatic axotomy.

Previously, we documented that suppressed expression of each of several Rab GTPases known to participate in synaptic vesicle cycling permitted enhanced axon regeneration (Sekine et al., 2018). This included Rab27b plus multiple Rab3 isoforms. Rph3a is known to function in synaptic vesicle recycling for this group of Rabs, and does so for axon regeneration as well, suggesting a shared cell biology amongst Rabs with respect to axon regeneration. Specifically, the effect of Rph3a loss is detected even when Rab27b is deleted and requires Rab3c. Because Rph3a mediates the action of more than one vesicular Rab in axon regeneration, its effect is more robust than that of Rab27b. Specifically, CST regeneration is detected for *Rph3a*$^{-/-}$, whereas only CST sprouting was observed in Rab27b null mouse SCI experiments with a less severe lesion.

While Rph3a mediates the axon regeneration effects of Rab27b and Rab3c, there is Rab-specificity with regard to upstream Rab GEFs. The protein MADD appears to act only through Rab27b since the axon regeneration effect of its knockdown is undetectable in neurons lacking Rab27b. Which GEFs interact with Rab3's with regard to axon regeneration and whether cell surface receptors drive GEF action will require further study.

The key role of Rab and Rab-related monomeric G proteins has been supported by several previous studies. The geranylgeranyl transferase is crucial for the prenylation and activity of this class of G proteins. Molecular screening studies with both small molecules and CRISPR gene editing have indicated a role for this Rab-modifying enzyme in axon growth (Li et al., 2016; Tian et al., 2019). The related G proteins, rab11 and arf6 (EFA6), has been documented to titrate integrin levels in the axon and thereby regulate axonal growth, with specific action of arf6 at the axon initial segment (Eva et al., 2012; Eva and Fawcett, 2014; Eva et al., 2017; Franssen et al., 2015; Koseki et al., 2017; Nieuwenhuis et al., 2018).

A priori, the role of Rab GTPases in coordinating membrane traffic might impact either bulk membrane delivery to the growth cone for axonal extension, or the distribution of key protein targets with critical roles in axonal growth. There is precedent for other axon growth regulators regulating bulk membrane traffic. In previous work, we found that inhibition of axonal extension by extracellular Semaphorin cues stimulates local macropinocytosis at the growth cone (Fournier et al., 2000). Loss of function for three endocytic genes in *C. elegans*, results in decreased regeneration (Chen et al., 2011). While the current data do not exclude a role for Rabs in direct regulation of bulk membrane addition, our studies provide direct evidence for Rph3a-selective regulation of cell surface integrin function. Because function-blocking ß1-integrin antibodies fully block the growth-promoting effect of Rph3a removal, the integrin signaling pathway is essential. While other cell surface receptors may also be altered, the action of Rph3a requires ß1-integrin signaling.

Integrin action is most commonly associated with the formation of focal adhesions and the regulation of filamentous actin dynamics. We show that loss of Rph3a increase FAK activation by biochemical and imaging measures in the axon tip, and modifies F-actin structures. Regenerating axons lacking Rph3a have more numerous F-actin-rich filopodia, with more rapid axon extension in live cell imaging studies. Our culture conditions likely contain multiple matrix ligands for ß1-integrins, so the most relevant integrin ligands *in vitro* and *in vivo* for regenerating axons remain to be defined.

It is notable that axotomy drives ß1-integrin association with Rph3a in regenerating axons. The axonal association of the two proteins becomes prominent only in the regenerating state. The molecular driver for this enhanced association is not yet clear. However, Rph3a is a calcium-binding protein, and axotomy is known to trigger substantial intra-axonal calcium ion increases. This provides a potential trigger for altered Rph3a association with integrins and endocytosis. In the absence of Rph3a, the same calcium trigger may fail to internalize integrins and instead integrin-FAK signaling may remain available to drive F-actin dynamics and advance the growth cone. Future studies measuring the rate of integrin delivery to the growth cone and the rate of integrin endocytic removal from the growth cone surface as a function of Rph3a level and regeneration will provide further insight. The action of both integrins and Rph3a on titrating axon regeneration are likely to depend on the extracellular matrix components to which growth cones adhere. Systematic investigation of substratum adherence should further delineate the actions of Rph3a in axon regeneration.

Our experiments focused on the role of Rph3a in regenerative growth from mature neurons and did not explore any potential role in developmental axon growth. However, we

demonstrate that the distribution of adult CST and raphespinal projections in the uninjured spinal cord of mice lacking Rph3a are indistinguishable from wild type, so any difference in developmental axon growth must be compensated or normalized over time. Our data demonstrate a specific role in neurons and axons, distinct from any potential role in glia or other cell types. While non-neuronal remains a theoretical possibility, the pattern of Rph3a expression in adult mouse brain is high in the vast majority of neuronal subtypes with little or no expression in glia (AllenBrainInstitute, 2022), supporting neuron-specific action. Furthermore, the deletion of Rph3a has no clear effect on astrocytic anti-GFAP staining or microcytic anti-Iba1 staining of the contused spinal cord (Wang and Strittmatter, unpublished observations).

The experiments here demonstrate greater axon regeneration in the absence of Rph3a for cultured neurons, for RGC axons in the optic nerve and for CST after spinal cord damage. Thus, the inhibitory role of Rph3a for axon regeneration may be widespread in adult mammalian CNS. In terms of behavioral outcome, the benefit of Rph3a deletion for spinal cord injury was limited. One potential explanation is that synapse function in the absence of Rph3a may be less than optimal. Any such impaired connectivity must be minimal since mice lacking Rph3a are without phenotype and synapse function is normal in the healthy *Rph3a*$^{-/-}$ CNS (Schlüter et al., 1999). However, there is evidence that synaptic recovery from use-dependent depression is regulated by Rph3a (Deak et al., 2006). Thus, recovery of function in *Rph3a*$^{-/-}$ mice may be limited by suboptimal synaptic function despite enhanced axon growth. Nonetheless, the current studies delineate a role for Rph3a in titrating integrins after axotomy and determining the extent of successful axon regeneration.

Supplementary Material

Refer to Web version on PubMed Central for supplementary material.

Acknowledgments

This work was supported by grants from the Falk Medical Research Trust and from the N.I.H. (R35NS097283) to S.M.S.

References

AllenBrainInstitute, 2022. ALLEN BRAIN MAP Transcriptomics Explorer.

Basso DM, Fisher LC, Anderson AJ, Jakeman LB, McTigue DM, Popovich PG, 2006. Basso mouse scale for locomotion detects differences in recovery after spinal cord injury in five common mouse strains. J. Neurotrauma 23, 635–659. [PubMed: 16689667]

Cai X, Lietha D, Ceccarelli DF, Karginov AV, Rajfur Z, Jacobson K, Hahn KM, Eck MJ, Schaller MD, 2008. Spatial and temporal regulation of focal adhesion kinase activity in living cells. Mol. Cell. Biol 28, 201–214. [PubMed: 17967873]

Chen MS, Huber AB, van der Haar ME, Frank M, Schnell L, Spillmann AA, Christ F, Schwab ME, 2000. Nogo-a is a myelin-associated neurite outgrowth inhibitor and an antigen for monoclonal antibody IN-1. Nature 403, 434–439. [PubMed: 10667796]

Chen L, Wang Z, Ghosh-Roy A, Hubert T, Yan D, O'Rourke S, Bowerman B, Wu Z, Jin Y, Chisholm AD, 2011. Axon regeneration pathways identified by systematic genetic screening in C. elegans. Neuron 71, 1043–1057. [PubMed: 21943602]

Deak F, Shin OH, Tang J, Hanson P, Ubach J, Jahn R, Rizo J, Kavalali ET, Sudhof TC, 2006. Rabphilin regulates SNARE-dependent re-priming of synaptic vesicles for fusion. EMBO J. 25, 2856–2866. [PubMed: 16763567]

Erturk A, Mauch CP, Hellal F, Forstner F, Keck T, Becker K, Jahrling N, Steffens H, Richter M, Hubener M, Kramer E, Kirchhoff F, Dodt HU, Bradke F, 2011. Three-dimensional imaging of the unsectioned adult spinal cord to assess axon regeneration and glial responses after injury. Nat. Med 18, 166–171. [PubMed: 22198277]

Eva R, Fawcett J, 2014. Integrin signalling and traffic during axon growth and regeneration. Curr. Opin. Neurobiol 27, 179–185. [PubMed: 24793179]

Eva R, Crisp S, Marland JR, Norman JC, Kanamarlapudi V, Ffrench-Constant C, Fawcett JW, 2012. ARF6 directs axon transport and traffic of integrins and regulates axon growth in adult DRG neurons. J. Neurosci 32, 10352–10364. [PubMed: 22836268]

Eva R, Koseki H, Kanamarlapudi V, Fawcett JW, 2017. EFA6 regulates selective polarised transport and axon regeneration from the axon initial segment. J. Cell Sci 130, 3663–3675. [PubMed: 28935671]

Fournier AE, Nakamura F, Kawamoto S, Goshima Y, Kalb RG, Strittmatter SM, 2000. Semaphorin3A enhances endocytosis at sites of receptor-F-actin colocalization during growth cone collapse. J. Cell Biol 149, 411–422. [PubMed: 10769032]

Fournier AE, GrandPre T, Strittmatter SM, 2001. Identification of a receptor mediating Nogo-66 inhibition of axonal regeneration. Nature 409, 341–346. [PubMed: 11201742]

Fournier AE, Gould GC, Liu BP, Strittmatter SM, 2002. Truncated soluble Nogo receptor binds Nogo-66 and blocks inhibition of axon growth by myelin. J. Neurosci 22, 8876–8883. [PubMed: 12388594]

Franssen EH, Zhao RR, Koseki H, Kanamarlapudi V, Hoogenraad CC, Eva R, Fawcett JW, 2015. Exclusion of integrins from CNS axons is regulated by Arf6 activation and the AIS. J. Neurosci 35, 8359–8375. [PubMed: 26019348]

Fukuda M, 2013. Rab27 effectors, pleiotropic regulators in secretory pathways. Traffic 14, 949–963. [PubMed: 23678941]

Geppert M, Bolshakov VY, Siegelbaum SA, Takei K, De Camilli P, Hammer RE, Sudhof TC, 1994. The role of Rab3A in neurotransmitter release. Nature 369, 493–497. [PubMed: 7911226]

GrandPre T, Nakamura F, Vartanian T, Strittmatter SM, 2000. Identification of the Nogo inhibitor of axon regeneration as a Reticulon protein. Nature 403, 439–444. [PubMed: 10667797]

Hu F, Strittmatter SM, 2008. The N-terminal domain of Nogo-a inhibits cell adhesion and axonal outgrowth by an integrin-specific mechanism. J. Neurosci 28, 1262–1269. [PubMed: 18234903]

Huebner EA, Kim BG, Duffy PJ, Brown RH, Strittmatter SM, 2011. A multidomain fragment of Nogo-a protein is a potent inhibitor of cortical axon regeneration via Nogo receptor 1. J. Biol. Chem 286, 18026–18036. [PubMed: 21454605]

Imai A, Ishida M, Fukuda M, Nashida T, Shimomura H, 2013. MADD/DENN/ Rab3GEP functions as a guanine nucleotide exchange factor for Rab27 during granule exocytosis of rat parotid acinar cells. Arch. Biochem. Biophys 536, 31–37. [PubMed: 23702376]

Jacquemet G, Stubb A, Saup R, Miihkinen M, Kremneva E, Hamidi H, Ivaska J, 2019. Filopodome mapping identifies p130Cas as a Mechanosensitive regulator of Filopodia stability. Curr. Biol 29 (202–216), e207.

Ji B, Li M, Budel S, Pepinsky RB, Walus L, Engber TM, Strittmatter SM, Relton JK, 2005. Effect of combined treatment with methylprednisolone and soluble Nogo-66 receptor after rat spinal cord injury. Eur. J. Neurosci 22, 587–594. [PubMed: 16101740]

Kannan R, Song JK, Karpova T, Clarke A, Shivalkar M, Wang B, Kotlyanskaya L, Kuzina I, Gu Q, Giniger E, 2017. The Abl pathway bifurcates to balance enabled and Rac signaling in axon patterning in Drosophila. Development (Cambridge, England) 144, 487–498.

Kim JE, Liu BP, Park JH, Strittmatter SM, 2004. Nogo-66 receptor prevents raphespinal and rubrospinal axon regeneration and limits functional recovery from spinal cord injury. Neuron 44, 439–451. [PubMed: 15504325]

Koseki H, Donega M, Lam BY, Petrova V, van Erp S, Yeo GS, Kwok JC, Ffrench-Constant C, Eva R, Fawcett JW, 2017. Selective rab11 transport and the intrinsic regenerative ability of CNS axons. Elife 6.

Kottis V, Thibault P, Mikol D, Xiao Z-C, Zhang R, Dergham P, Braun PE, 2002. Oligodendrocyte-myelin glycoprotein (OMgp) is an inhibitor of neurite outgrowth. J. Neurochem 82, 1566–1569. [PubMed: 12354307]

Lee JK, Kim JE, Sivula M, Strittmatter SM, 2004. Nogo receptor antagonism promotes stroke recovery by enhancing axonal plasticity. J. Neurosci 24, 6209–6217. [PubMed: 15240813]

Li S, Liu BP, Budel S, Li M, Ji B, Walus L, Li W, Jirik A, Rabacchi S, Choi E, Worley D, Sah DW, Pepinsky B, Lee D, Relton J, Strittmatter SM, 2004. Blockade of Nogo-66, myelin-associated glycoprotein, and oligodendrocyte myelin glycoprotein by soluble Nogo-66 receptor promotes axonal sprouting and recovery after spinal injury. J. Neurosci 24, 10511–10520. [PubMed: 15548666]

Li S, Kim JE, Budel S, Hampton TG, Strittmatter SM, 2005. Transgenic inhibition of Nogo-66 receptor function allows axonal sprouting and improved locomotion after spinal injury. Mol. Cell. Neurosci 29, 26–39. [PubMed: 15866044]

Li H, Kuwajima T, Oakley D, Nikulina E, Hou J, Yang WS, Lowry ER, Lamas NJ, Amoroso MW, Croft GF, Hosur R, Wichterle H, Sebti S, Filbin MT, Stockwell B, Henderson CE, 2016. Protein Prenylation constitutes an endogenous brake on axonal growth. Cell Rep. 16, 545–558. [PubMed: 27373155]

Lindborg JA, Tran NM, Chenette DM, DeLuca K, Foli Y, Kannan R, Sekine Y, Wang X, Wollan M, Kim IJ, Sanes JR, Strittmatter SM, 2021. Optic nerve regeneration screen identifies multiple genes restricting adult neural repair. Cell Rep. 34, 108777. [PubMed: 33657370]

Liu BP, Fournier A, GrandPre T, Strittmatter SM, 2002. Myelin-associated glycoprotein as a functional ligand for the Nogo-66 receptor. Science 297, 1190–1193. [PubMed: 12089450]

McKeon RJ, Schreiber RC, Rudge JS, Silver J, 1991. Reduction of neurite outgrowth in a model of glial scarring following CNS injury is correlated with the expression of inhibitory molecules on reactive astrocytes. J. Neurosci 11, 3398–3411. [PubMed: 1719160]

Mizoguchi A, Yano Y, Hamaguchi H, Yanagida H, Ide C, Zahraoui A, Shirataki H, Sasaki T, Takai Y, 1994. Localization of Rabphilin-3A on the synaptic vesicle. Biochem. Biophys. Res. Commun 202, 1235–1243. [PubMed: 8060298]

Moore DL, Blackmore MG, Hu Y, Kaestner KH, Bixby JL, Lemmon VP, Goldberg JL, 2009. KLF family members regulate intrinsic axon regeneration ability. Science 326, 298–301. [PubMed: 19815778]

Nieuwenhuis B, Haenzi B, Andrews MR, Verhaagen J, Fawcett JW, 2018. Integrins promote axonal regeneration after injury of the nervous system. Biol. Rev. Camb. Philos. Soc 93, 1339–1362. [PubMed: 29446228]

Park KK, Liu K, Hu Y, Smith PD, Wang C, Cai B, Xu B, Connolly L, Kramvis I, Sahin M, He Z, 2008. Promoting axon regeneration in the adult CNS by modulation of the PTEN/mTOR pathway. Science 322, 963–966. [PubMed: 18988856]

Ruschel J, Hellal F, Flynn KC, Dupraz S, Elliott DA, Tedeschi A, Bates M, Sliwinski C, Brook G, Dobrindt K, Peitz M, Brustle O, Norenberg MD, Blesch A, Weidner N, Bunge MB, Bixby JL, Bradke F, 2015. Axonal regeneration. Systemic administration of epothilone B promotes axon regeneration after spinal cord injury. Science 348, 347–352. [PubMed: 25765066]

Schlüter OM, Schnell E, Verhage M, Tzonopoulos T, Nicoll RA, Janz R, Malenka RC, Geppert M, Südhof TC, 1999. Rabphilin Knock-out mice reveal that Rabphilin is not required for Rab3 function in regulating neurotransmitter release. J. Neurosci 19, 5834–5846. [PubMed: 10407024]

Schwab ME, Strittmatter SM, 2014. Nogo limits neural plasticity and recovery from injury. Curr. Opin. Neurobiol 27, 53–60. [PubMed: 24632308]

Sekine Y, Lin-Moore A, Chenette DM, Wang X, Jiang Z, Cafferty WB, Hammarlund M, Strittmatter SM, 2018. Functional genome-wide screen identifies pathways restricting central nervous system axonal regeneration. Cell Rep. 23, 415–428. [PubMed: 29642001]

Shen Y, Tenney AP, Busch SA, Horn KP, Cuascut FX, Liu K, He Z, Silver J, Flanagan JG, 2009. PTPsigma is a receptor for chondroitin sulfate proteoglycan, an inhibitor of neural regeneration. Science 326, 592–596. [PubMed: 19833921]

Shirataki H, Kaibuchi K, Yamaguchi T, Wada K, Horiuchi H, Takai Y, 1992. A possible target protein for smg-25A/rab3A small GTP-binding protein. J. Biol. Chem 267, 10946–10949. [PubMed: 1597436]

Smith PD, Sun F, Park KK, Cai B, Wang C, Kuwako K, Martinez-Carrasco I, Connolly L, He Z, 2009. SOCS3 deletion promotes optic nerve regeneration in vivo. Neuron 64, 617–623. [PubMed: 20005819]

Stanic J, Carta M, Eberini I, Pelucchi S, Marcello E, Genazzani AA, Racca C, Mulle C, Di Luca M, Gardoni F, 2015. Rabphilin 3A retains NMDA receptors at synaptic sites through interaction with GluN2A/PSD-95 complex. Nat. Commun 6 10181. [PubMed: 26679993]

Tedeschi A, Dupraz S, Curcio M, Laskowski CJ, Schafffan B, Flynn KC, Santos TE, Stern S, Hilton BJ, Larson MJE, Gurniak CB, Witke W, Bradke F, 2019. ADF/Cofilin-mediated actin turnover promotes axon regeneration in the adult CNS. Neuron 103 (1073–1085), e1076.

Tian R, Gachechiladze MA, Ludwig CH, Laurie MT, Hong JY, Nathaniel D, Prabhu AV, Fernandopulle MS, Patel R, Abshari M, Ward ME, Kampmann M, 2019. CRISPR interference-based platform for multimodal genetic screens in human iPSC-derived neurons. Neuron 104 (239–255), e212.

Tolmachova T, Abrink M, Futter CE, Authi KS, Seabra MC, 2007. Rab27b regulates number and secretion of platelet dense granules. Proc. Natl. Acad. Sci. U. S. A 104, 5872–5877. [PubMed: 17384153]

Wang X, Baughman KW, Basso DM, Strittmatter SM, 2006. Delayed Nogo receptor therapy improves recovery from spinal cord contusion. Ann. Neurol 60, 540–549. [PubMed: 16958113]

Wang X, Duffy P, McGee AW, Hasan O, Gould G, Tu N, Harel NY, Huang Y, Carson RE, Weinzimmer D, Ropchan J, Benowitz LI, Cafferty WB, Strittmatter SM, 2011. Recovery from chronic spinal cord contusion after Nogo receptor intervention. Ann. Neurol 70, 805–821. [PubMed: 22162062]

Wang X, Yigitkanli K, Kim CY, Sekine-Komo T, Wirak D, Frieden E, Bhargava A, Maynard G, Cafferty WB, Strittmatter SM, 2014. Human NgR-fc decoy protein via lumbar intrathecal bolus administration enhances recovery from rat spinal cord contusion. J. Neurotrauma 31, 1955–1966. [PubMed: 24964223]

Wang X, Zhou T, Maynard GD, Terse PS, Cafferty WB, Kocsis JD, Strittmatter SM, 2020. Nogo receptor decoy promotes recovery and corticospinal growth in non-human primate spinal cord injury. Brain 143, 1697–1713. [PubMed: 32375169]

Yoshimura S, Gerondopoulos A, Linford A, Rigden DJ, Barr FA, 2010. Family-wide characterization of the DENN domain Rab GDP-GTP exchange factors. J. Cell Biol 191, 367–381. [PubMed: 20937701]

Zhang Z, Fujiki M, Guth L, Steward O, 1996. Genetic influences on cellular reactions to spinal cord injury: a wound-healing response present in normal mice is impaired in mice carrying a mutation (WldS) that causes delayed Wallerian degeneration. J. Comp. Neurol 371, 485–495. [PubMed: 8842901]

Zukor K, Belin S, Wang C, Keelan N, Wang X, He Z, 2013. Short hairpin RNA against PTEN enhances regenerative growth of corticospinal tract axons after spinal cord injury. J. Neurosci 33, 15350–15361. [PubMed: 24068802]

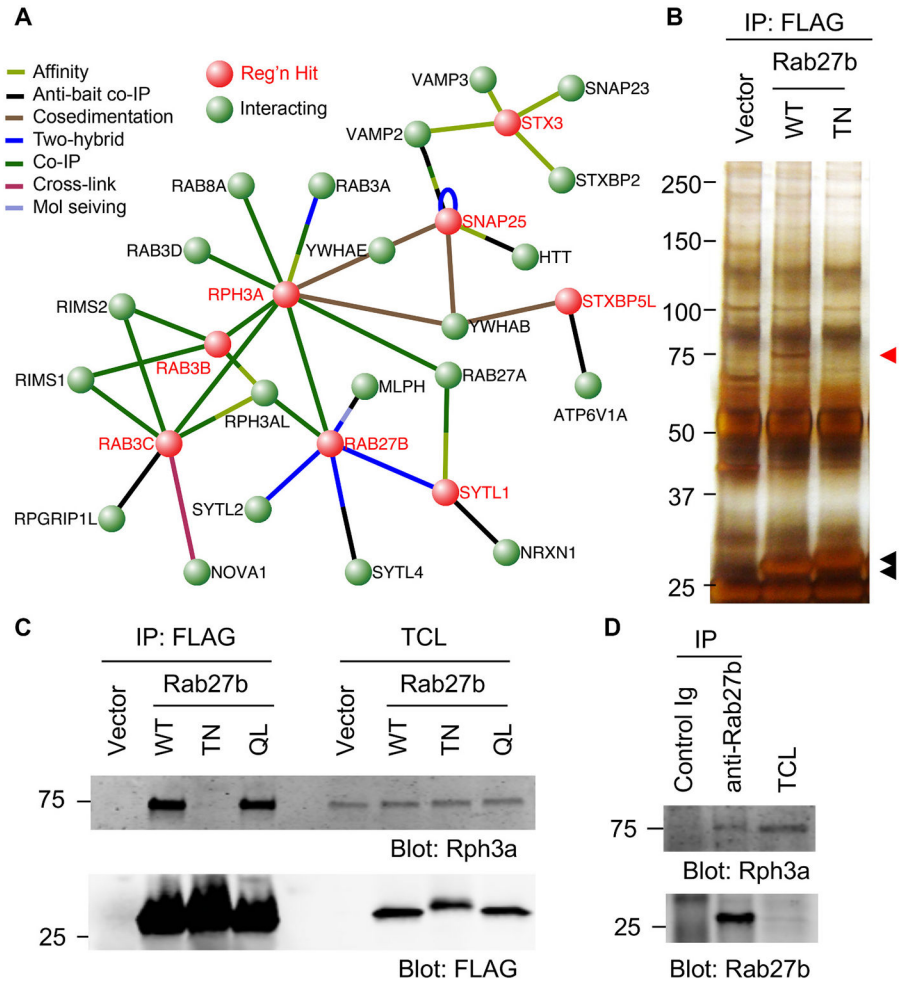

Fig. 1. Rph3a is a Rab27b effector.

(A) Rab27b Network related to Axon Regeneration. Protein-protein interaction network of mouse proteins connected to Rab27b from Visant website. The nodes in red were each hits in the primary regeneration screen(Sekine et al., 2018). Rab27b is direct binding partner for Rph3a and Sytl1. The evidence for protein-protein intereaction is shown by colour of the edges.

(B) Cortical neurons were nucleofected with vector, Rab27b WT or T23N. On DIV 10, neurons were lysed and immunoprecipitated with anti-FLAG antibody. The immune complexes were then resolved by SDS-PAGE and silver stained. Red arrow shows a band in Rab27b WT lane for MS. Black arrows are immunoprecipitated FLAG-Rab27b WT and TN.

(C) Cortical neurons were nucleofected with vector, Rab27b WT, T23N or Q78L. On DIV10, neurons were lysed and immunoprecipitated with anti-FLAG antibody. The immune complexes were then resolved by SDS-PAGE and immunoblotted with ant-Rph3a and FLAG antibodies.

(D) DIV 10 cortical neurons were lysed and immunoprecipitated with control or anti-Rab-27b antibody. The immune complexes were then resolved by SDS-PAGE and immunoblotted with anti-Rph3a and Rab27b antibodies.

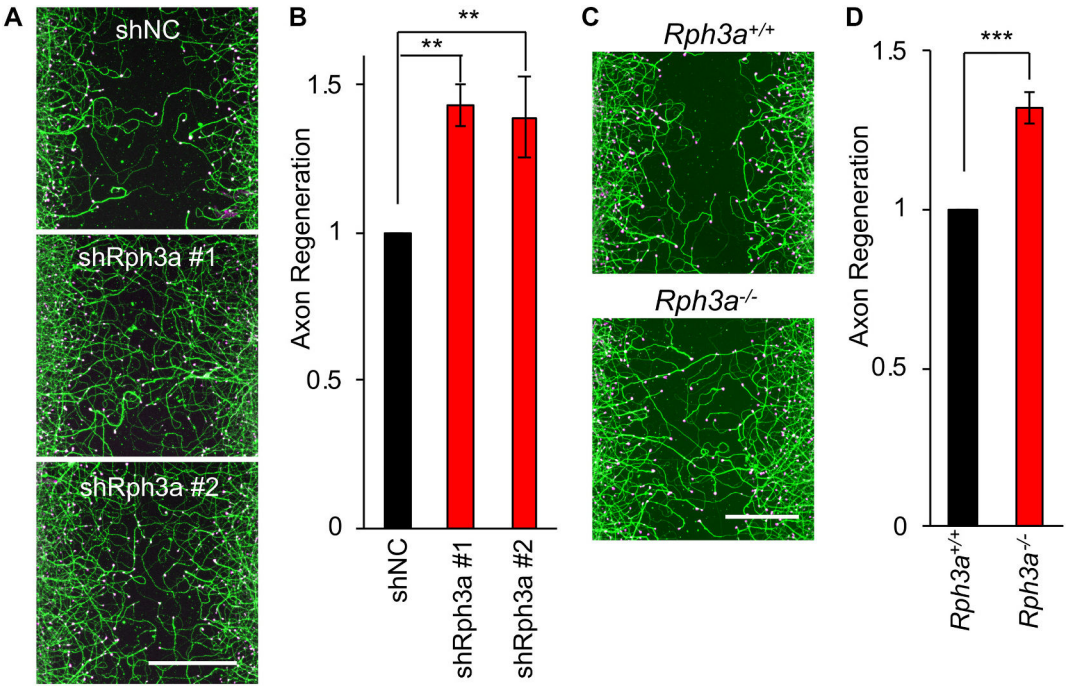

Fig. 2. Suppression of Rph3a expression enhances axonal regeneration *in vitro*.

(A) Representative pictures of regenerated axons nucleofected with shNC, shRph3a #1 or #2 in cortical neurons. The microphotographs show ßIII-tubulin (in axons; green) and phalloidin (to stain F-actin; magenta) to illustrate the growth cones of cortical neurons in the middle of the scraped area. Scale bars represent 200 μm.

(B) The graph shows quantification of axonal regeneration relative to shNC. Mean ± SEM, n = 3 biological replicates. **p < 0.01, one-way ANOVA followed by Tukey's test (F = 13.85, dF = 2,).

(C) Representative pictures of regenerated axons in WT and Rph3a$^{-/-}$ cortical neurons. The microphotographs show ßIII-tubulin (in axons; green) and phalloidin (to stain F-actin; magenta) in the middle of the scraped area. Scale bars represent 200 μm.

(D) The graph shows quantification of axonal regeneration relative to WT neuron. Mean ± SEM, n = 3 biological replicates. ***p < 0.005, Student *t*-test (t = 6.885, dF = 4).

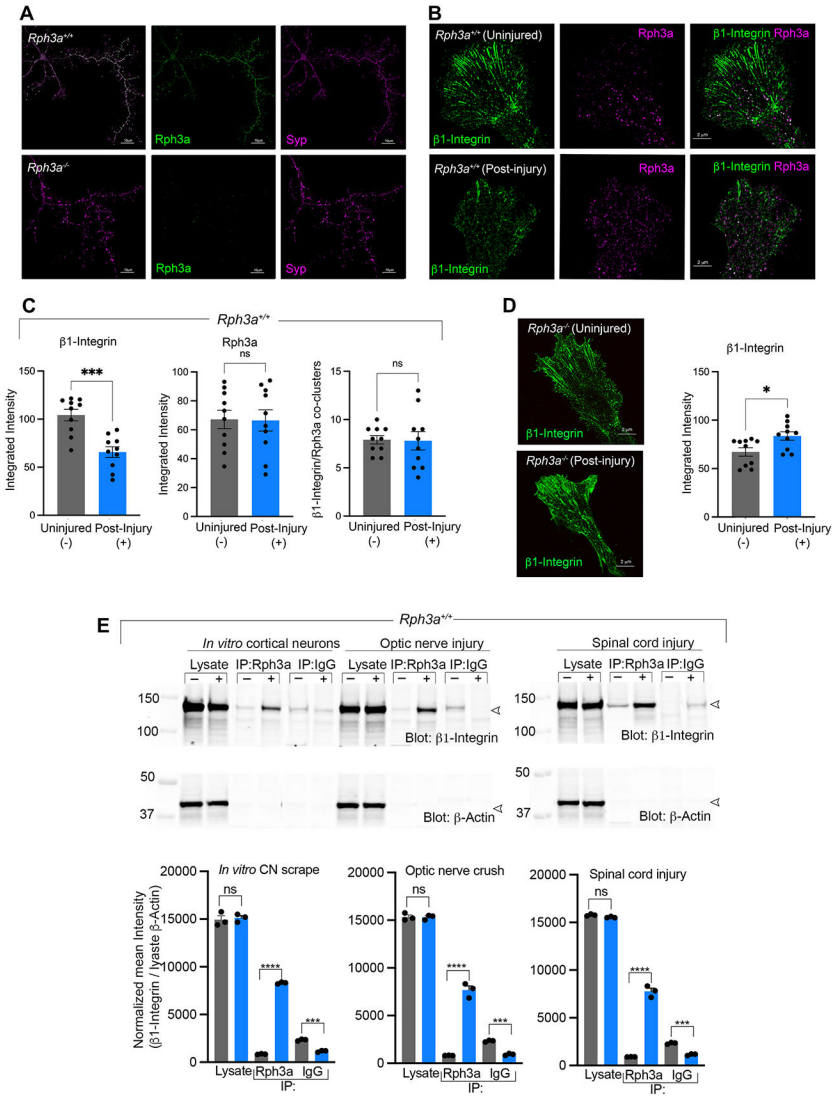

Fig. 3. Rph3a regulates integrin post-axotomy.

(A) Representative Airyscan images of *Rph3a*$^{+/+}$ and *Rph3a*$^{-/-}$, 7DIV cortical neurons. Immunofluorescent localization of Rph3a (green) with the vesicle membrane marker synaptophysin (Syp, magenta) is shown. Scale bar, 10 μm.

(B) Representative Airyscan images of axonal growth cones from *Rph3a*$^{+/+}$ at 8–9 DIV, 2–3 days post-axotomy. Localization of Rph3a shown in magenta and ß1-Integrin in green. Scale bar, 2 μm.

(C) Quantitative image analysis of cultures as in (B). Graphs represent integrated intensity of ß1-Integrin, Rph3a pixels and the number of ß1-Integrin/Rph3a coclusters in the growth cones. Data are mean ± SEM from individual growth cones of three independent cultures. For ß1-Integrin (***p < 0.001; t = 4.7; df = 17.8); Rph3a (p = 0.942; t = 0.07; df = 17.6) and Integrin/Rph3a coclusters (p = 0.92; t = 0.09; df = 12.5) by unpaired Student t-test with Welch correction.

(D) Representative Airyscan images showing ß1-Integrin localization in axonal growth cones from *Rph3a*$^{-/-}$ at 8-9DIV, 2–3 days post-axotomy. Graph represents ß1-Integrin

integrated intensity under both conditions. Data are mean ± SEM from individual growth cones of three independent replicate cultures. *p = 0.016; $t = 2.6$; df = 18 by unpaired Student t-test with Welch correction. Scale bar 2 μm.

(E) Protein extracts from *in vitro* cortical neurons, optic nerve, and spinal cord of *Rph3a*$^{+/+}$, 7 days post-axotomy were analyzed by immunoprecipitation (IP). Control (−, gray bars) and axotomized (+, blue bars) lysates were immunoprecipitated with anti-Rph3a or control IgG and probed for anti-ß1-Integrin and ß-actin by immunoblot. Densitometry analysis of immunoblots from 3 replicates are summarized and presented as mean ± SEM. ***p = 0.0003, ****p < 0.0001 (CNs: F = 1120, Df = 17; ONC: F = 1053, Df = 17; SCI: F = 2245, Df = 17), one-way ANOVA with Sidak's multiple comparison test.

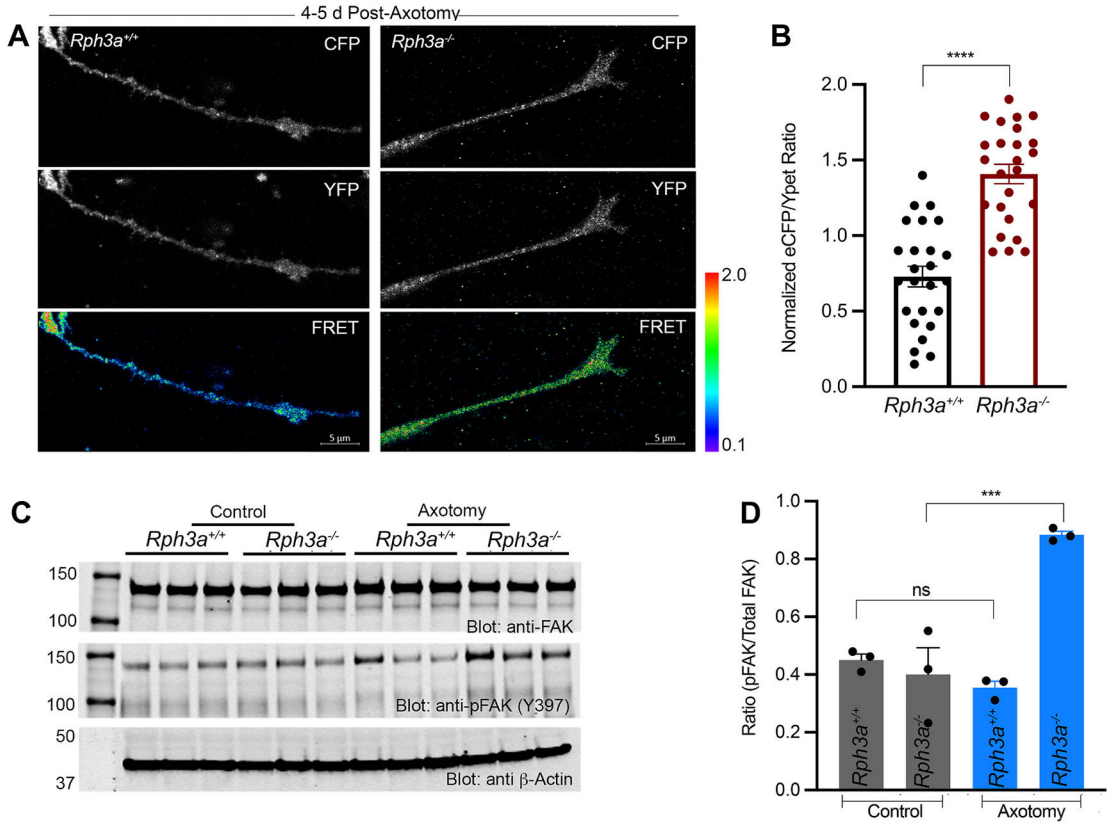

Fig. 4. Increased FAK activation in regenerating *Rph3a*$^{-/-}$ growth cones.

(A) Prototypical ECFP/YPet ratio, ECFP and YPet images of FAK biosensor expressed transiently in regenerating axons of *Rph3a*$^{+/+}$ and *Rph3a*$^{-/-}$ cortical neurons, 4–5 days post-axotomy. Pseudo colour scale for FRET signal is shown with limiting values for each genotype. Scale bar, 5 µm.

(B) Bar graph represents ECFP/YPet emission ratio values (mean + SEM) quantified from regenerating axons of *Rph3a*$^{+/+}$ (n = 25) and *Rph3a*$^{-/-}$ (n = 25) from three independent replicates. ****p < 0.0001 (t = 7.216, Df = 48), from unpaired Student t-test.

(C) Protein extracts from *Rph3a*$^{+/+}$ and *Rph3a*$^{-/-}$ 4–5 days post-axotomy cortical neurons were immunoblotted for p-FAK against total FAK levels, respectively. bactin used as internal loading control.

(D) Densitometry analysis of p-FAK immune blot. Ratio of p-FAK to total FAK from three independent cultures. ***p = 0.002 (F = 24.58, Df = 11) by one-way ANOVA with Sidak's multiple comparison test statistic.

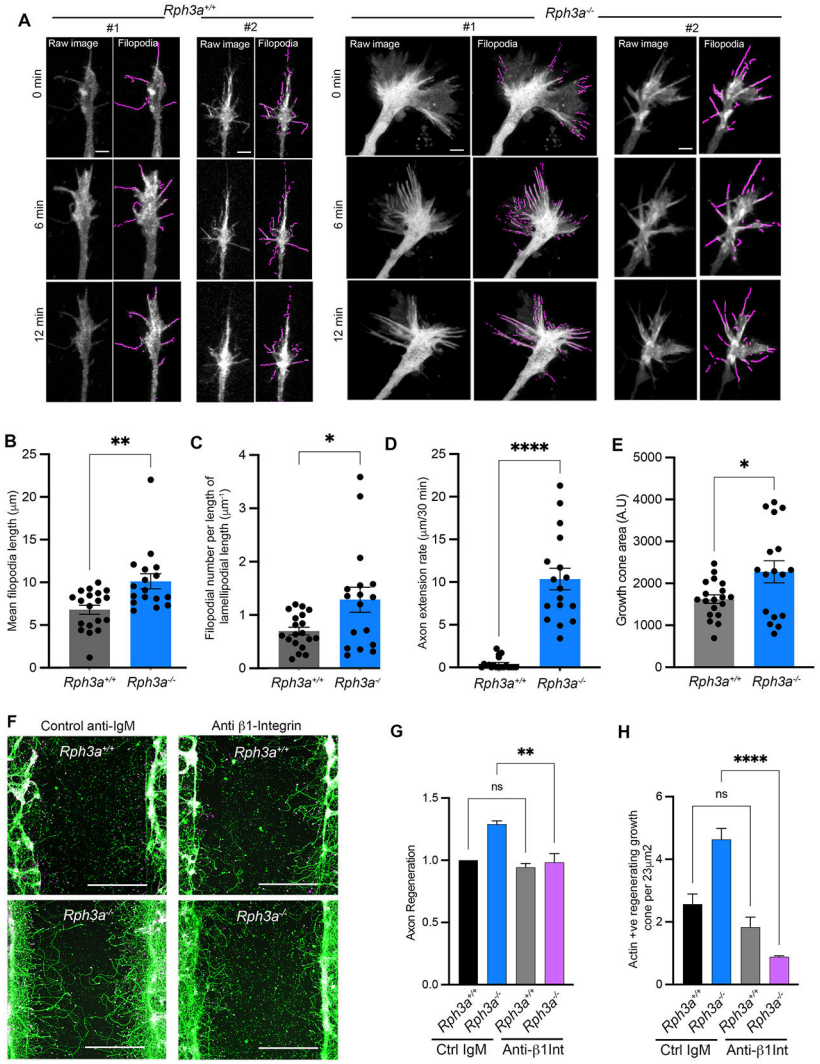

Fig. 5. Increased filopodia and integrin-dependent axon extension of regenerating *Rph3a*$^{-/-}$ growth cones.

(A) Time lapse imaging of regenerating growth cones of cortical neurons from *Rph3a*$^{+/+}$ (n = 19) and *Rph3a*$^{-/-}$ (n = 17), 5–7 days post axotomy. Cortical neurons were transfected with Life Act-mScarlet to label F-actin rich filopodial structures. Maximum intensity *z*-projection for three time points were shown for each genotype. Left are raw images used for automatic filopodia detection, highlighted in purple. Scale bar, 5 μm.

(B) Quantification of filopodial length for 30 min time-lapse, mean ± SEM for individual growth cones from 3 biological replicates. **p = 0.0035 (U = 71), by non-parametrie Mann-Whitney test.

(C) The ratio of filopodial number to the edge length of lamellipodia, mean ± SEM. *p = 0.0415 (U = 92), by non-parametric Mann-Whitney test.

(D) The rate of axon extension over 30 min time-lapse window, mean ± SEM. ****p < 0.0001 (U = 0), by non-parametric Mann-Whitney test.

(E) Area of regenerating growth cones from experiment as in A. *p < 0.05 (U = 0), by non-parametric Mann-Whitney test.

(F) Integrin Function-Blocking Antibody prevents axonal regeneration of *Rph3a*$^{-/-}$ neurons. Representative images of *Rph3a*$^{+/+}$ and *Rph3a*$^{-/-}$ regenerated axons, 7 days post-axotomy, treated with ß1-Integrin function-blocking antibody and its respective isotype control. Cortical neurons were stained for ßIII-tubulin (green) and phalloidin (magenta) to label regenerating axons and actin-rich growth cones.

(G and H) Graphs represent quantification of axonal regeneration and actin-rich regenerating growth cones. Data plotted are normalized mean values ± SEM from n = 3 biological replicates with a total of ~200,000 neurons/treatment/experiment. One-way ANOVA with Sidak's (for F) and Tukey's multiple comparison test (for G) statistic applied. **p = 0.0042 (F = 15.21, Df = 11), ****p < 0.0001 (F = 30.3, Df = 11). Scale bar, 200 μm.

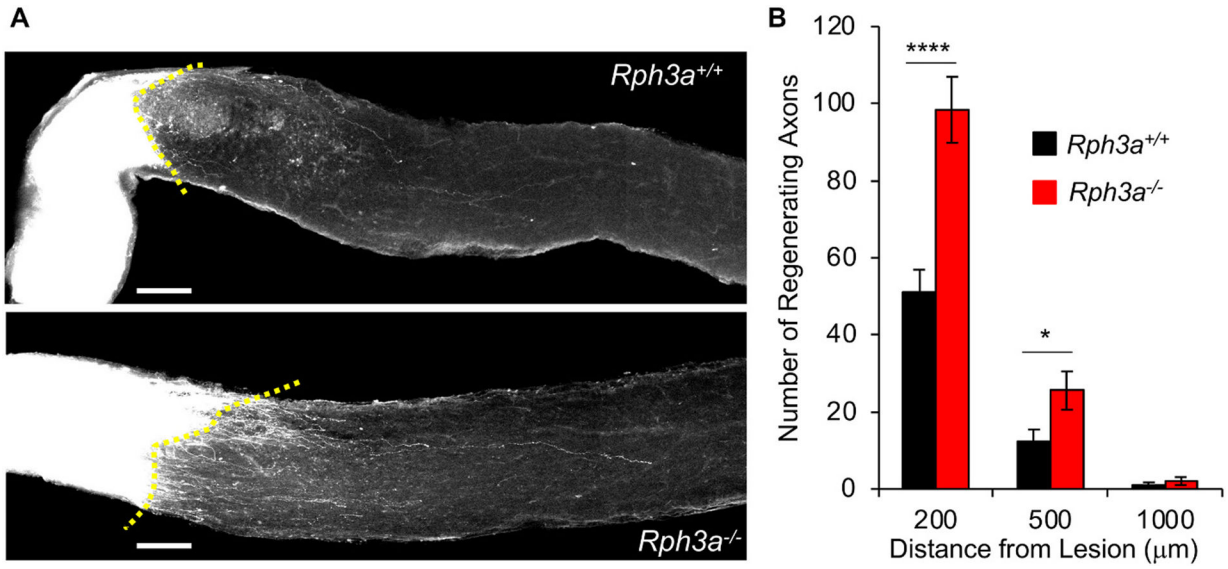

Fig. 6. Rph3a inhibits retinal ganglion cell axonal regeneration *in vivo*.

(A) Representative confocal images of optic nerve at 17 days after crush injury from wild type control mouse and *Rph3a*$^{-/-}$ mouse. The CTB-labeled RGC axons are white. The eye is the left and the brain to the right. Scale bars represent 100 μm.

(B) Quantification of regenerating axons at 200, 500 and 1000 μm distances distal to the lesion sites at 17 days after injury. Data are mean ± SEM for n = 20 *Rph3a*$^{+/+}$ and n = 13 *Rph3a*$^{-/-}$. By repeated-measure ANOVA, $p < 0.0001$ for genotype effect ($F = 21.49$, $dF = 1$), *$p < 0.05$ ($F = 5.66$, $dF = 1$,), ****$p < 0.0001$ ($F = 22.46$, $dF = 1$) for indicated pairs by one-way ANOVA.

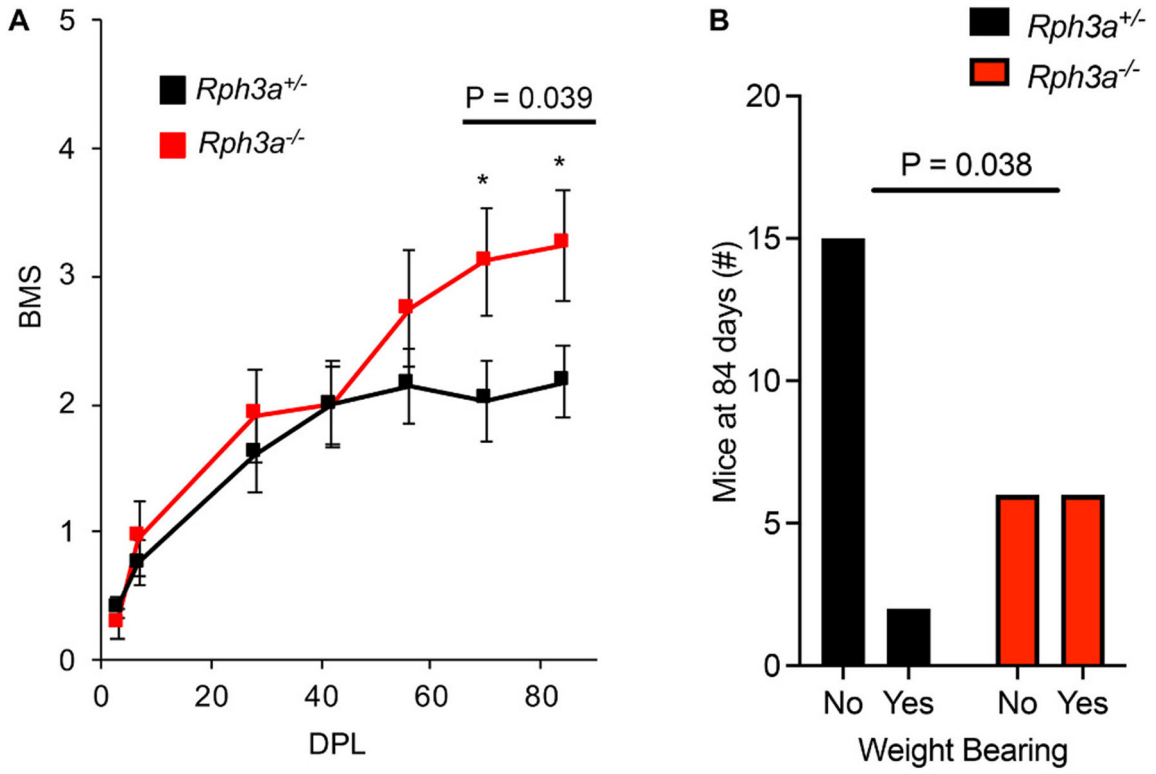

Fig. 7. Improvement of functional recovery after SCI in *Rph3a*$^{-/-}$ mice.

(A) Open-field locomotion performance assessed by BMS of *Rph3a*$^{+/-}$ and *Rph3a*$^{-/-}$ mice. Animals were scored on day post lesion (DPL) −3, 3, 7, 28, 42, 56, 70 and 84 by two experienced observers blinded of group. Data are mean ± SEM for n = 17 *Rph3a*$^{+/-}$ and n = 12 *Rph3a*$^{-/-}$. *p = 0.039, repeated-measure ANOVA for group effect across last two time points (F = 4.71, dF = 1), and *p < 0.05 (F = 4.40, dF = 1 and F = 4.635, dF = 1), significant difference between indicated pairs by one-way ANOVA.

(B) Weight bearing of *Rph3a*$^{+/-}$ and *Rph3a*$^{-/-}$ mice on DPL 84. Data report weight bearing status of mice in each group. n = 17 *Rph3a*$^{+/-}$ and n = 12 *Rph3a*$^{-/-}$. Fisher's Exact contingency test, *p = 0.038.

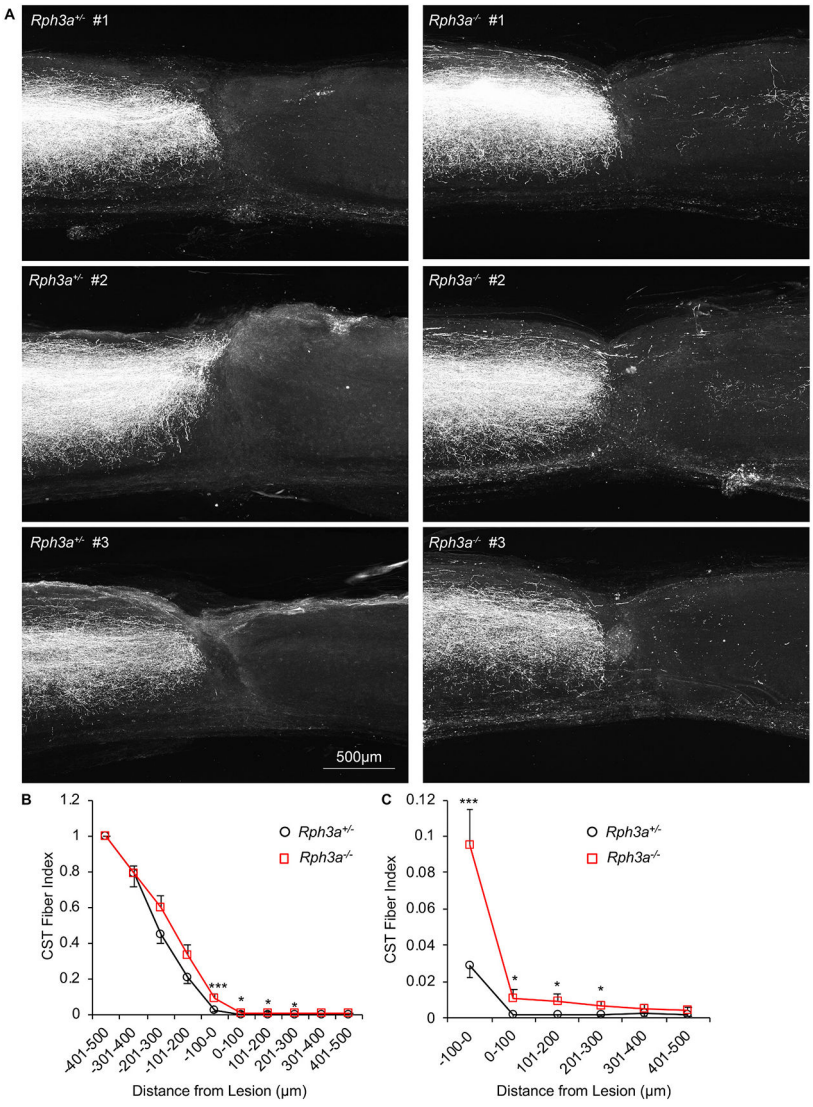

Fig. 8. Enhanced corticospinal axonal regeneration in *Rph3a*$^{-/-}$ mice after SCI.

(A) Representative confocal images of BDA labeled CST axons around the lesion site. The BDA labeled axons are white. All sections were overlaid. Dorsal is up and rostral is left. Scale bar represents 500 μm.

(B) Quantification of regenerating axons rostral (−500 μm) and caudal (500 μm) to the epicenter of the lesion site. The number of BDA-positive axons at indicated area is counted from all sections per animal. Data are mean ± SEM for n = 17 *Rph3a*$^{+/-}$ and n = 12 *Rph3a*$^{-/-}$. By repeated-measure ANOVA, ***p = 0.001 (F = 12.48, dF = 1), for genotype effect between 100 μm rostral to 300 μm caudal, *p < 0.05 (F = 5.41, dF = 1, F = 4.50, dF = 1 and F = 4.69, dF = 1), ***p < 0.001 (F = 13.02, dF = 1) for indicated pairs by one-way ANOVA.

(C) High magnification graph of (B) between −100 to 500 μm.

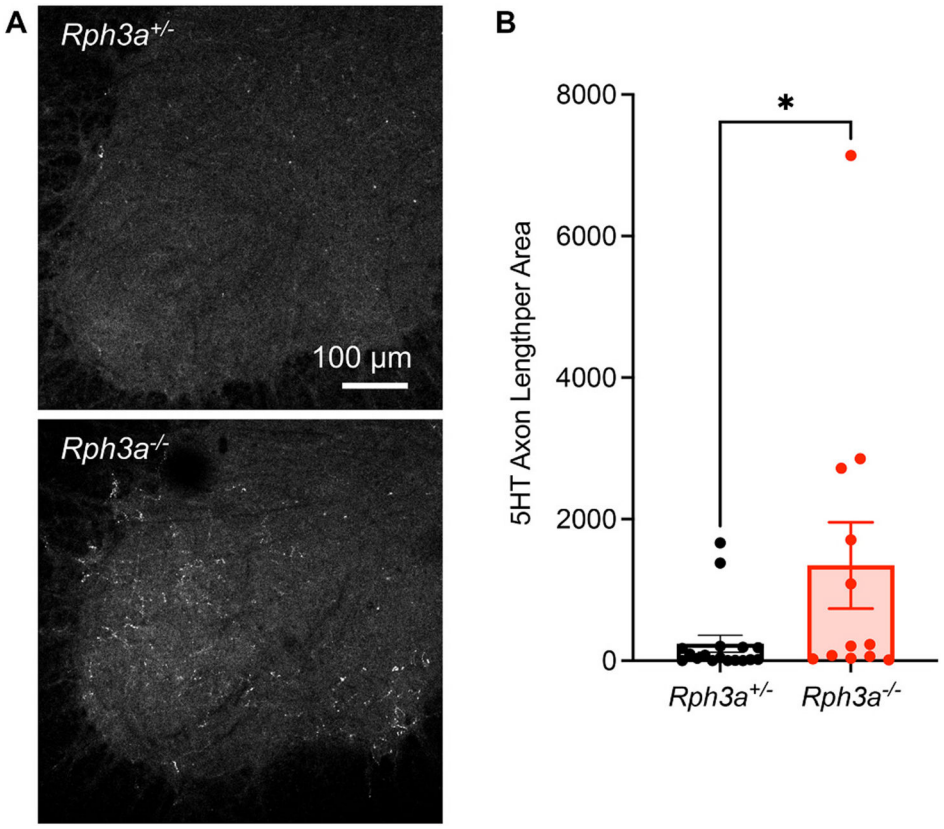

Fig. 9. Increased raphespinal axon growth after SCI in *Rph3a*$^{-/-}$ mice.

(A) Representative image of raphespinal fibers stained with anti-5HT antibody in the spinal ventral horn at caudal to the lesion. Scale bar represents 100 µm.

(B) Quantification of serotonergic 5HT+) fiber length per unit area in the lumbar ventral horn caudal to the lesion site from *Rph3a*$^{+/-}$ and *Rph3a*$^{-/-}$ mice 84 days after SCI. Data are mean with SEM for n = 17 *Rph3a*$^{+/-}$ and n = 12 *Rph3a*$^{-/-}$. *p < 0.05 (U = 53.50), non-parametric Mann-Whitney *U* test for non-normal distribution.

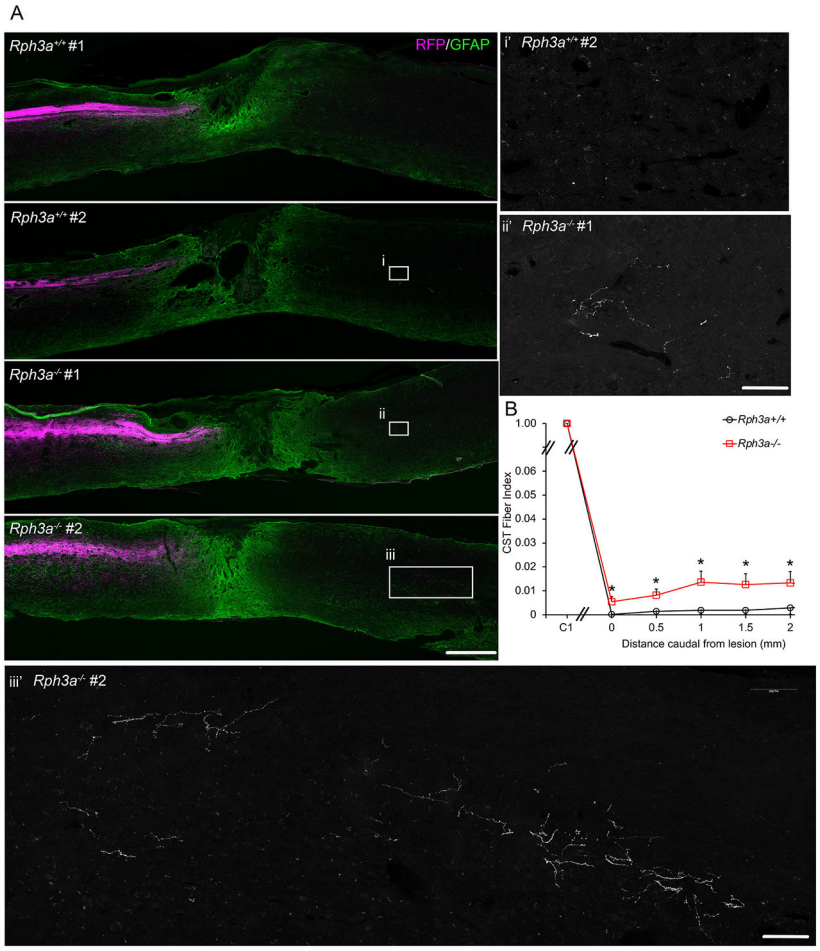

Fig. 10. Enhanced CST regeneration in *Rph3a*$^{-/-}$ mice after spinal contusion.

(A) Representative images of longitudinal section of lesion segment of spinal cord from the *Rph3a*$^{-/-}$ and WT mice with spinal contusion injury at T9 spinal level, stained with anti-RFP (magenta) and anti-GFAP (green) antibodies. Rostral is to the left and dorsal is up. Scale bar =500 μm. Boxed areas in i, ii and iii are magnified in i', ii' and iii' for the RFP channel only. RFP-labeled CST fibers increased in the *Rph3a*$^{-/-}$ animals. Scale bar is 100 μm in i', ii' and iii'.

(B) Quantification of RFP-labeled CST axons in spinal cord caudal to lesion. RFP positive fibers are reported as a function of caudal distance relative to the SCI lesion site in the *Rph3a*$^{-/-}$ knockout group (n = 7) as compared to the WT group (n = 7). Data are mean ± SEM. *p < 0.05 (p = 0.023, F = 6.83, dF = 1), repeated-measure ANOVA for group effect across all sites, and *p < 0.05 (p = 0.028, F = 6.20, dF = 1; p = 0.032, F = 5.88, dF = 1; p = 0.027, F = 6.29, dF = 1; p = 0.044, F = 5.09, dF = 1; and p = 0.050, F = 4.74, dF = 1), significant difference between indicated pairs by one-way ANOVA.